A calibrated surface complexation model for carbonate-oil-brine interactions coupled with reservoir simulation- application to controlled salinity water flooding

Lawrence Opoku Boampong, Roozbeh Rafati*, Amin Sharifi Haddad

School of Engineering, University of Aberdeen, Aberdeen, United Kingdom, AB24 3UE

Abstract

Vast majority of past studies that have been conducted on controlled salinity water flooding (CSWF) use diffuse layer model (DLM) that calculates only the surface potential, which can be significantly different from the ζ-potential of the interface. Importantly, stability of the water-film (between the oil and the rock surface) which dictates ultimate oil recovery is related to ζ-potential. As such, using DLM calculated surface potential (directly) for CSWF can be misleading. Additionally, most of the existing DLMs use integer charges instead of fractional charges to model carbonate-brine interactions, which may not represent the actual carbonate crystallographic. We present a triple layer surface complexation model (TLM) which offers the option to locate and distribute charge of the adsorbing ion(s) at three locations. TLM can therefore calculate potentials at three different locations within the Stern layer. To the best of our knowledge, only few authors have used TLM to simulate CSWF. However, some surface reactions were ignored in these models. For instance, adsorption of monovalent ions such as Na^+ and Cl^- ions was ignored in some of the few available TLMs. Also, the effect of basic-oil components was not considered in some TLMs, and lastly, some TLMs used integer charges for the carbonate surface group. This study introduced a comprehensive TLM that includes all these complexities. Moreover, we introduced a new wettability indicator (WI) that is related to the electrostatic forces between the oil-brine and the rock-brine interfaces. That is, WI was calculated from ζ-potentials at the oil-brine and rock-brine interfaces.

The TLM, built in a geochemical simulator, PHREEQC, was then coupled with UTCHEM, a multiphase reservoir simulator. The developed simulator based on the TLM-CSWF model was tested against several experimentally measured oil recovery data sets. Results of the model suggest that Oil basic component significantly impacts oil-brine interface ζ-potential irrespective of temperature, brine composition, and ionic strength. On the otherhand, Na^+ ions in brine may influence oil-brine ζ-potential, and this relates to temperature, brine composition, and ionic strength. The results further suggest that injection of (sulfate-free) diluted brine in chalk resulted to increased oil adhesion, shifting the reservoir to oil-wet condition. Hence, no additional oil is recovered with this brine injected at tertiary oil recovery stage. Finally, the results showed that wettability is related to ζ-potentials at the oil-brine and rock-brine interfaces, and the carbonate rock would be strongly oil-wet or water-wet only at significantly large magnitude of ζ-potentials at the interfaces.

Keywords: Low salinity water flooding, Disjoining pressure, Electrical double layer, Wettability alteration, Zeta potential, Controlled salinity water flooding.

1. Introduction

CSWF was observed in 1959 when Martin[1] identified higher oil production from fresh water injection in sandstone. It was, however, not recognized until Morrow et al.[2–4] began to do deeper investigation. Currently, many researchers and industries are working tremendously to get more insight into this EOR method. Although there have been numerous reported cases of positive impact of CSWF on oil recovery[2–7], and laboratory experiments show that high recovery is related to CSWF compared to conventional water flooding, however, the underlying mechanism behind the process is not well understood and still opens for further research. In recent years, several mechanisms behind the improved oil recovery have been proposed with some researchers either confirming or refuting them. Studies conducted so far associate the improved oil recovery to wettability alteration in carbonate reservoirs. It is stated that the introduction of CSW into the reservoir induces water-rock-oil interactions which results to wettability alteration[8].

It has been proposed that the wettability alteration is related to the water film stability subject to electrical charges that are generated at the oil-brine and rock-brine interfaces[6,9–12]. Therefore, brine, which is capable of generating same polarities of ζ-potential at the oil-brine and rock-brine interface will produce a more stable water film between the oil and the rock surface, making the reservoir water wet. Alternatively, Austad et al.[7]; Fathi et al.[13]; Strand et al.[14] and Zhang et al.[15,16] proposed multi-component ion exchange as the mechanism behind the wettability alteration in carbonate reservoirs. They indicated that adsorption of some specific ions (Ca^{+2}, Mg^{+2}, SO_4^{-2}) can lead to desorption of adsorbed oil from the rock surface, which shifts the reservoir to water-wet state. Other proposed mechanisms responsible for the wettability alteration include rock dissolution[17,18] and interfacial tension reduction[19].

Successful works have proven that improved oil recovery is not exclusively caused by the total dissolved salt, but specific composition and concentrations of the wettability-altering species in the injection water [5,7]. The interaction between reservoir rocks and fluids, focusing on ionic composition and salinity has been studied by several authors. It was established that rock-brine-oil interaction (i.e.: wettability alteration) is controlled predominantly by pH and potential determining ions (PDI) such as $Ca^{2+,}$ Mg^{2+}, CO_3^{-2}, SO_4^{2-}, and the presence or absence of these ions dictates the amount of oil that can be recovered by CSWF[7,8,16,20–25]. Ligthelm et al.[26], on the other hand, reported that wettability alteration is effective when ionic strength is lowered rather than the action of PDI. Some researchers have also argued that CSWF is complex and explaining it with a single mechanism is difficult[18,27,28].

1.1. Theory of electrical double layer (EDL) and zeta potential (ZP)

When a carbonate rock comes into contact with an electrolyte solution, the chemical state of the carbonate surface is usually altered. This leads to the separation of electrical charge at the carbonate-solution interface[29]. An excess of charge at the carbonate surface is balanced through electrostatic interaction with counter-ions, which are attracted from the adjacent solution to the carbonate surface[10,29]. This generates first layer at the mineral surface, which is often referred to as the Stern layer. Subsequently, a second layer is generated around the first layer because it could not completely neutralize the surface. This second layer is termed as diffuse layer, and the two layers, together, is called electrical double layer (Figure 1a). It

should be noted that the diffuse layer contains both counter-ions and co-ions, with the co-ions concentration increasing towards the bulk electrolyte solution. It is worth mentioning that the ions in the Stern layer are strongly adhered to the surface and are compact while the ions in the diffuse layer are mobile[10].

The Stern layer can further be divided into two as inner Helmoltz layer and outer Helmoltz layer. Thus, inner Helmoltz layer refers to the region between the 0-plane and the inner Helmoltz plane (IHP) whereas outer Helmoltz layer is the region between the IHP and the outer Helmoltz plane (IHP). While 0-plane denotes the hydrolysis layer (where OH^- and H^+ are chemi-bonded to the surface ions), IHP defines location of dehydrated ions that are closely attached to the surface. The OHP, however, defines locations of hydrated ions[29,30] that are far from the surface. The IHP and the OHP can also be referred to as 1-plane and 2-plane, respectively. The Helmoltz layers can be described as capacitors with capacitances C1 (capacitance between the 0-plane and the 1-plane) and C2 (capacitance between the 1-plane and the 2-plane). The electric potential within the EDL varies with distance from the surface (Figure 1b), and the potential obtained at the slip plane is called zeta ζ-potential (Figure 1b).

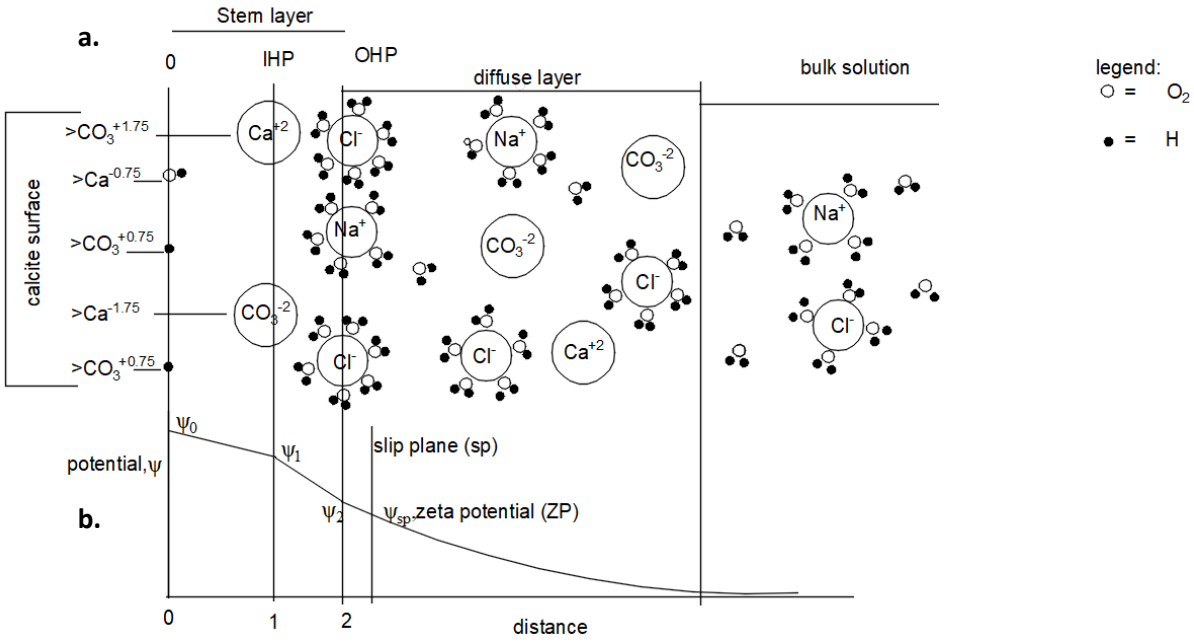

Figure 1: (a) sketch of the electrical double layer at the carbonate-brine interface. The stern layer is described by three planes: the 0-plane which denotes the hydrolysis layer where OH^- and H^+ are chemi-bonded to the surface ions; the 1-plane which is location for adsorbed ions closer to the surface; and the 2-plane which is location for adsorbed ions farther from the surface (b) Schematic representation of electrical potential variation with distance from the rock surface[29,30]. The charges deposited at the calcite surface are results of the rock interactions with the electrolyte ions.

1.2. Stability of the water film between the oil and reservoir rock

In oil reservoirs, contact between the rock surface and oil is dictated by the stability of the water film between the oil and the rock surface[11]. If the water film is unstable, then, oil can easily adhere to the rock surface, making the reservoir oil-wet or mixed-wet (Figure 2a). The water film stability is dictated by the disjoining pressure existing between the rock and the

fluids. In other word, disjoining pressure can be described as the force that tends to separate the oil-brine and rock-brine interfaces. It should be noted that a negative disjoining pressure attracts the two interfaces[31], making the reservoir oil-wet (Figure 2b).

Three forces, namely, van der Waals forces (VDWF), structural forces (SF) and double layer forces (DLF) of electrostatic in nature contribute to the disjoining pressure. The summation of these force components is expressed as the total disjoining pressure[10,31]. For oil-brine-rock system, VDWF is always considered attractive (i.e.: negative contribution to DP) while SF is repulsive. On the other hand, DLF can be attractive or repulsive depending on the polarities of ζ-potential at the oil-brine and rock-brine interfaces. For instance, if the oil-brine and rock-brine interfaces have the same polarity, DLF will be repulsive, and its contribution to DP will be positive. This suggests that it is the DLF which dictates DP and water film stability.

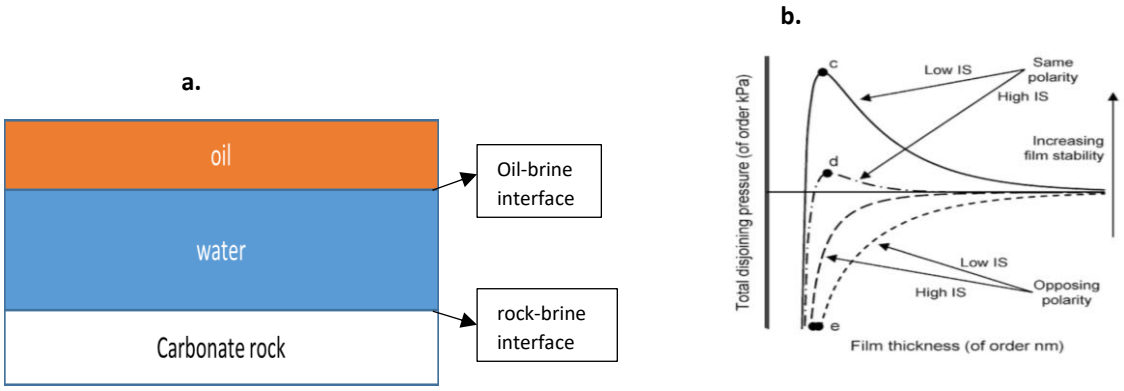

Figure 2: schematic representation of: (a) rock-brine-oil system in equilibrium; (b) disjoining pressure isotherm (Jackson et al.[6]). "c" in the disjoining pressure isotherm denotes stable water-film at low ionic strength; "d" is partially stable water-film at high ionic strength; and "e" is unstable water-film. Conditions "c" and "d" occur under same polarities of ζ-potential at the oil-brine and rock-brine interfaces whereas condition "e" denotes opposite ζ-potential at the interfaces. High ionic strength reduces magnitude of ζ-potential and double layer thickness, thus, DP can be reduced. "IS" in Figure b signifies ionic strength.

1.3. Surface complexation model (SCM) for CSWF

Surface complexation models have been used to characterize crude oil-rock-brine (CORB) interactions in the reservoir[5,10,17,18,23,32–48]. They have the capability to describe surface adsorption/desorption phenomena of CORB using chemical reactions, mass balance, charge balance and equilibrium constants[49]. Some available SCM includes basic Stern model, BSM (Figure 3b), diffuse layer model, DLM (Figure 3a) and triple layer model, TLM (Figure 3c). It should be noted that each model differs from the other in its structural representation of mineral-solution interface. That is, location and configuration of adsorbed species at the surface[49]. Vast majority of past studies that have been conducted on CSWF use DLM[5,17,23,32,42,50–52], which calculates only the potential at the surface (0-plane). It is noteworthy that surface potential can be significantly different from the ζ-potential. Importantly, stability of the water-film which dictates ultimate oil recovery is related to ζ-potential. As such, using DLM calculated surface potential (directly) for CSWF can be misleading. Therefore, DLM calculated potential needs to be modified in order to estimate ζ-potential. That is, a correlation such as Debye-Huckel approximation or Gouy-Chapmann relation is applied to estimate ζ-potential from DLM calculated surface potential. However,

Debye-Huckel approximation is valid at low potential values (surface potential < 25mV), which limits its application. Furthermore, with asymmetrical solution, complex equations are required to calculate ζ-potential from the surface potential (Israelachvili.[53]). BSM, on the other hand, assumes that protonation/deprotonation reactions take place at the 0-plane, while all adsorption reactions of ions from the bulk electrolyte take place at the b-plane. In other words, BSM does not distinguish the Stern layer as IHP and OHP. BSM has been used by some investigators to model rock-brine interactions[54,55]. TLM, on the other hand, relies on the theory that charges are distributed on the 0-plane, the IHP and OHP, which could result in a ζ-potential value that is calculated directly from the model itself rather than using correlations to find the ζ-potential as the diffuse layer models require.

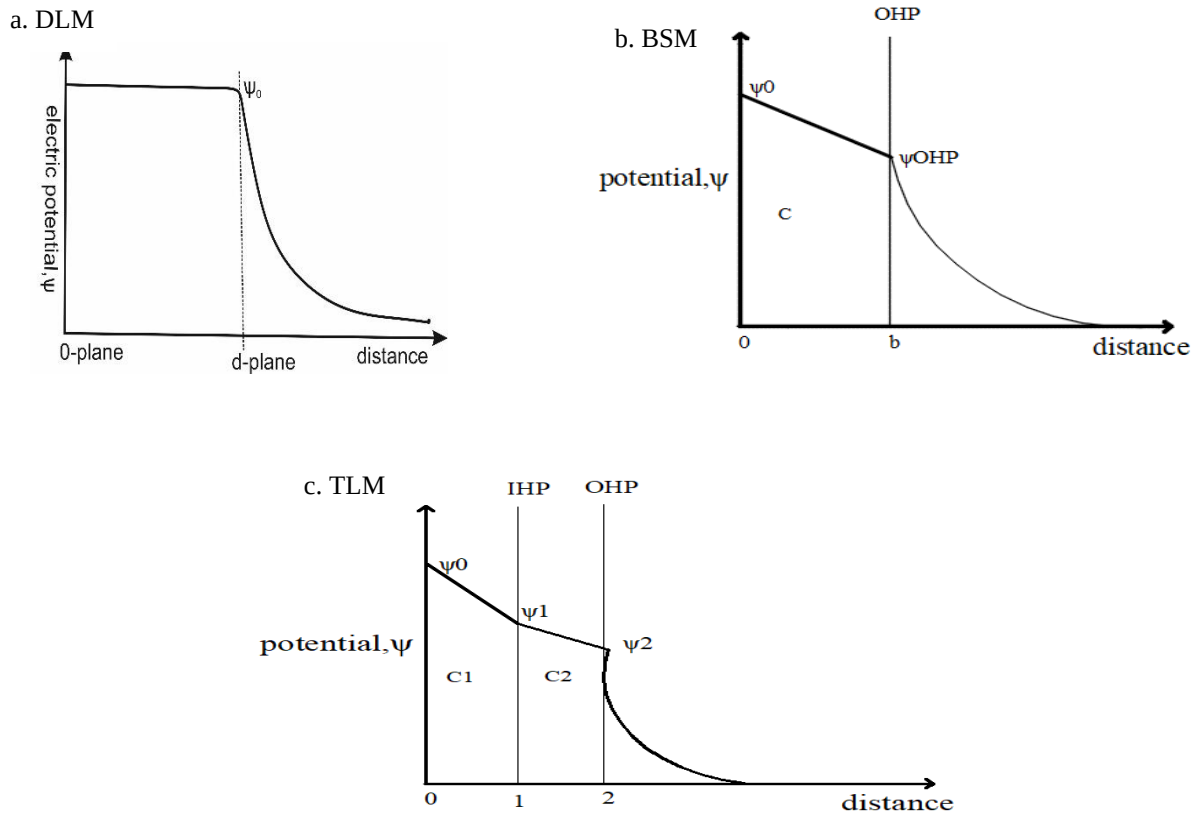

Figure 3: (a) schematic representation of diffuse layer model: It comprises of an empty stern layer and a diffuse layer. Electric potential remains constant from the surface till the onset of the diffuse layer (d-plane), where it begins to decrease exponentially with distance. (b) Sketch of BSM: It does not separate the Stern layer into IHP and OHP. (c) Sketch of TLM: The stern layer is described by three planes: the '0-plane', the IHP (1-plane), and the OHP (2-plane). It requires two capacitance values (C1 and C2) and distribution of its electric potential is consistent with the EDL theory.

TLM has been used successfully to model rock-brine interactions (in environmental studies) by several researchers[30,56–60]. Stipp[61], through a study conducted on carbonate-brine interactions indicated that the charge obtained at the calcite lattice ions (>Ca and $>CO_3$) is not an integer but rather a fraction. Stipp[61] further mentioned that the charge is ± 0.333 if the bond is pure ionic. This suggests that using integer charges to model carbonate interactions may not represent the actual carbonate crystallographic. TLM is capable of modelling carbonate-brine reactions which involve fractional charges. Moreover, the distribution of

TLM electric potential is consistent with the electrical double layer (EDL) theory. To the best of our knowledge, only few studies have reported the use of TLM to model CORB interactions and CSWF oil recovery process. Recently, Bonto et al.[41] modelled CSWF but used TLM for the carbonate-brine interactions and DLM for the oil-brine interactions. In addition, their TLM was validated with only one experimental result. Takeya et al.[37,38] also used TLM to model CORB interactions, however, some oil-brine surface reactions were ignored in the model. Additionally, there is limited literature on oil-brine SCM, and most of the available ones use equilibrium constants at 25^{o}C to model the reactions at various temperatures. Subsequently, a new improved model that can incorporate all these factors is needed to effectively characterise CORB interactions and CSWF process.

This study seeks to develop a comprehensive SCM that is capable of modelling and predicting CORB interactions at different temperatures, brine composition/salinity, carbonate mineralogy and oil composition. A TLM was made from Charge-Distribution Multi-site Complexation (CD-MUSIC) built in PHREEQC. We included all the above discussed factors in the developed SCM. In modelling CSWF, the effect of the CSW on oil recovery is simulated via a shift in relative permeability using wettability interpolant (WI). Past papers have proposed various WI models which includes bond product sum (BPS)[39,40,62,63], stability number (SN)[64], available adsorption site[41], concentration of adsorbed oil species at the rock surface[32,33]. It is interesting to note that reliability of some of these proposed WI have been questioned by some authors as they failed to predict oil recovery trend. For instance, Korrani et al[64] did not observe correlation between oil recovery and BPS as this WI failed to predict most of the simulated oil recovery data. Also, SN showed no correlation with oil recovery when utilised by Bonto et al[41] to simulate CSWF data. We introduced a new WI that is related to the electrostatic forces between the oil-brine and the rock-brine interfaces. That is, this WI was calculated from ζ-potentials at the oil-brine and rock-brine interfaces. The SCM model was then coupled with a reservoir simulator, UTCHEM, to simulate CSWF oil recovery in carbonate reservoirs. Finally, the model was verified by matching it to several experimentally measured ζ-potential and oil recovery data sets.

2. Methodology

A TLM model that calculates oil-brine and carbonate-brine interactions is introduced in the study. The model is made from CD-MUSIC, which is a powerful tool for modelling solid-solution interactions. The TLM is coupled with UTCHEM to simulate CSWF in carbonate porous media. The method developed in this study includes three steps:

a. Modelling carbonate-brine and oil-brine ζ-potentials: PHREEQC is used to simulate ζ-potentials at the oil-brine and rock-brine interfaces. This was achieved by matching the model to several oil-brine and rock-brine experimentally measured ZP data sets
b. Modelling CSWF: low salinity waterflooding was simulated using a reservoir simulation package, UTCHEM, coupled with PHREEQC. This coupled model is referred to as TLM-CSWF model
c. Model validation with published CSWF data sets: the TLM-CSWF model was validated with experimentally measured CSWF data sets

2.1. Modelling carbonate-brine and oil-brine zeta potential

Equilibrium constants and capacitances were estimated for oil-brine and carbonate-brine interactions separately. Oil-brine interaction parameters were first estimated followed by carbonate-brine reaction parameters.

2.1.1. Estimating oil-brine reaction equilibrium constants and capacitances

a. Oil surface site density determination

Buckley et al.[11] indicated that the active surface sites at the oil-brine interface are the acidic and basic components in the crude oil. Two sites, namely, acid site and base site were therefore considered. It should be pointed out that oil acid site-density (N_{COOH}) and base site-density (N_{NH}) were calculated from the total acid number (TAN) and total base number (TBN) of the oil, respectively, using Equation (1 - 2)[41,64,65]:

$$N_{COOH}\left(\frac{no.\ sites}{nm^2}\right) = 0.602 \times 10^6 \times \frac{TAN(mgKOH/g\ oil)}{1000 \times a_{oil \times MW_{KOH}}} \quad (1)$$

$$N_{NH}\left(\frac{no.\ sites}{nm^2}\right) = 0.602 \times 10^6 \times \frac{TBN(mgKOH/g\ oil)}{1000 \times a_{oil \times MW_{KOH}}} \quad (2)$$

Where: a_{oil} denotes oil specific surface area in m^2/g, and MW_{KOH} is the molecular weight of KOH, and 0.602×10^6 is a conversion factor from mol/m^2 to no. sites/nm^2. The TAN and TBN, therefore, are input parameters for acidic and basic sites-densities determination. In this study, we assumed an oil specific surface area of 1.0 m^2/g.[40,64]

***b. Locating and distributing charge of the adsorbed ion at the oil-brine interface*:**

Electrolyte ions interacting with the oil surface have various sizes, and as a result, these ions may be located at different distances from the oil surface[66]. Protonation/deprotonation reactions were assumed to occur in the 0-plane[30,37,41,55] whereas other sorption reactions were modelled to take place at the 1-plane[37,41]. Charge change occurring in the 0-plane (i.e.: Z0) and 1-plane (i.e.: Z1) due to the sorption reaction is calculated using Equations 3 and 4[57]:

$$Z0 = \Delta n_H V_H + f V_{me} \quad (3)$$

$$Z1 = (1 - f) V_{me} + \sum m_i z_i \quad (4)$$

where Δn_H denotes change in proton at the surface, V_H is valence of the proton, $V_{me}\ is$ valence of central atom in the aqueous complex, m_i denotes number of ligands present in the 1-plane, z_i is charge of those ligands in the 1-plane and f is charge distribution fraction, which accounts for fraction of V_{me} distributed to the 0-plane. In most cases, the adsorbed ions are treated as point charges, as such; their overall charge is deposited at one specific plane. Consequently, f = 0. Based on Taketa et al.[37], we assigned the charge of the adsorbed ion to one plane. For instance, the total charge (+2) of Ca^{+2} ion is assumed to be centered at the 1-plane in the Stern layer. Hence, charge change, Z1 at the 1-plane is +2 whereas charge change, Z0 at the 0-plane is -1 (due to loss of one proton from the oil surface).

c. Capacitance values:

Previous SCM for carbonate rocks have used large capacitance values. One of such models is the constant capacitance model developed by Cappellen et al.[67]; where high capacitance value was used for the carbonate-brine interface. Constant capacitance models, similar to BSM require only one capacitance value. Wolthers et al.[30] also used high capacitance values of 100F/m^2 for both C1 (capacitance between the 0-plane and the 1-plane) and C2 (capacitance between the 1-plane and the 2-plane) in their TLM model. However, such high capacitance values are deemed to be unrealistic and unreasonable with their usage being challenged by some authors, including, Heberling et al[55]. They argued that such high capacitance values would give a Stern layer thickness below 1.0$\dot{A}$. Sø et al.[58], when employed C1 and C1 values of 100F/m^2 in their TLM, the modelled sorption isotherms were all straight while the experimental isotherms were strongly curved. Heberling et al.[55] indicated that the total capacitance, C_T of the Stern layer should be within the range between 0.1 F/m^2 and 2.8 F/m^2. Some recent SCM have utilized low values of C1 and C2 consistent with the range of values proposed by Heberling et al[55]. Bonto et al.[41] used C1 = 1.3F/m^2 and C2 = 4.5F/m^2 for a carbonate-brine TLM. Sø et al.[58] also employed constant C2 value of 4.5F/m^2 while varying C1 within the range between 1.3 – 3.0F/m^2. Li et al (2010) (cited in Sø et al.[58]) estimated C1 and C2 values of 2.8F/m^2 and C2 4.5F/m^2, respectively for calcite. Based on Li et al's, we used C1 = 2.8 F/m^2 and C2 = 4.5 F/m^2. Although, capacitance values might change at different temperatures, but to reduce the number of tuning parameters the above mentioned capacitances were used in the entire work. Moreover, Wolthers et al[30] and Sø et al[58,59] did not observe significant change in the potentials calculated from variations in the capacitance values.The optimized oil-brine interface reaction parameters are shown by Table 1.

Table 1: optimized oil-brine interface reaction parameters. Z0, Z1, correspond to charge change at the 0 and 1 planes, respectively. The enthalpy change was calculated using Van't Hoff equation.

No.	Reactions	log_K at: 25ºC	50ºC	Z0	Z1	$\Delta H°$, KJ/mol
1	>RCOOH <=> >RCOO$^-$ + H$^+$	-4.8	-4.5	-1	0	22.13
2	>N + H <=> >NH$^+$	3.92	3.5	1	0	-30.99
3	>RCOOH + Na$^+$ <=> >RCOONa + H$^+$	-4.2	-4.52	-1	1	-23.61
4	>RCOOH + Ca^{+2} <=> >RCOOCa$^+$ + H$^+$	-3.1	-3.63	-1	2	28.04
5	>RCOOH + Mg^{+2} <=> >RCOOMg$^+$ + H$^+$	-3.58	-3.2	-1	2	-39.1
6	C1, F/m^2	2.8				
7	C2, F/m^2	4.5				

d. ζ-potential estimation

Following other investigators [30,37,41,42,68], we computed ζ-potential assuming that slip plane coincides with the OHP.[68]. That is, ζ-potential = ψ_{OHP}, where ψ_{OHP} is the potential at the outer Helmoltz plane calculated by PHREEQC. Hereafter, we matched our model 2-plane potential to the experimentally measured ζ-potential data sets.

2.1.2. Estimating carbonate-brine reaction equilibrium constants and capacitances

a. Carbonate surface site density determination

Two calcite lattice ions, calcium (>Ca) and carbonate (>CO_3) were considered at the calcite-water interface. Following Stipp[61], fractional charge of 0.25 was assumed for calcite (>$Ca^{+0.25}$; >$CO_3^{-0.25}$) in this study. Bonto et al.[41] and Wolthers et al.[30] assumed fractional charge of 0.667 while Heberling et al.[54] used fractional charge of 0.5. Song et al.[69] on the other hand, assumed fractional charge of 0.25, consistent with Stipp[61]. It should be emphasized that the total surface charge density is not affected by the magnitude of the fractional charge[54]. When calcite is in contact with aqueous solution, its surface sited get hydrated and then protonation/deprotonation reactions take place at 0-plane to yield two new complexes >$CaOH^{-0.75}$ and >$CO_3H^{+0.75}$. Consequently, these principal surface sites; >$CaOH^{-0.75}$, >$CaOH_2^{+0.25}$, >$CO_3H^{+0.75}$, and >$CO_3^{-0.25}$ were used in our model. Moreover, it was assumed that site-density equals 4.95 sites/nm^2 for each site[54,69]. Based on Brady & Krumhansi[70] and Heberling et al.[54], specific surface area was set to 1.0m^2/g.

b. Locating and distributing charge of the adsorbed ion at the rock-brine interface

Similar to the oil-brine interface model, protonation/deprotonation reactions were assumed to occur in the 0-plane, with other sorption reactions occurring in the 1 and 2 planes. One major challenge in SCM is identifying location of the adsorbing ions in the Stern layer. While some authors assume and place all the adsorbing ions either in the 1-plane or the 2-plane, others distribute them between the 1- and 2-planes. For instance, Rahnemaie et al.[56] specified that monovalent ions such as Cl^-, Na^+ have weak interactions with mineral surfaces, and these ions are adsorbed at the OHP. Bonto et al.[41]; and Sø et al.[58], however, modelled all the adsorbing ions at the IHP. Heberling et al.[55], on the contrary, modelled all the adsorbing ions at the OHP in their developed BSM. Wolthers et al.[30] ran sensitivity analysis by simulating CO_3^{-2}, Ca^{+2} and HCO_3^- sorption at the IHP. In another model, the ions were simulated at the OHP. However, potentials calculated from the two models were similar. Takeya et al.[53] on the other hand, assumed that Na^+ and Cl^- ions are adsorbed in the diffuse layer whiles divalent ions are adsorbed at the IHP. In this study, Na^+ and Cl^- ions adsorptions are modelled at the OHP, whereas divalent ions adsorption is modelled at the IHP. Charge change in the planes (i.e.: Z0, Z1) as a result of the sorption reactions are calculated with equations 4 and 5. Also, charge change occurring in the 2-plane (i.e.: Z2) is calculated using equation 5.

Regarding CO_3^{-2}, SO_4^{-2} adsorption, part of the adsorbed species is incorporated into the calcite surface (0-plane) through ligand exchange, whereas the remaining part is present in the 1-plane[57]. Consequently, charge of central atom in these ions is distributed between the 0-plane and the 1-plane. Wolthers et al.[30] assumed that f = 0.4, and further proposed that the value of f does not significantly affect the modelling results. Based on Sø et al.[58], f was set to 0.24 in this study. For instance, considering monodentate adsorption of CO_3^{-2} ion (>$CaOH^{-0.75}$ + CO_3^{-2} <=> >$CaCO_3^{-1.75}$ + OH^-); $Z0 = (-1 \times 1) + (0.24 \times 4) = -0.04$; $Z1 = (1 - 0.24) \times (4) + (2 \times (-2) = -0.96$. On the other hand, the charge of adsorbed Ca^{+2}, Mg^{+2}, Cl^- and Na^+ was assigned to one plane, as such , f = 0.

c. Capacitance values

The capacitance values used for the oil-brine interface reaction calculations are used for the modelling of rock-brine interface reactions. That is C1 = 2.8 F/m^2 and C2 = 4.5 F/m^2. The optimized carbonate-brine interface reaction parameters are given by Table 2.

Table 2: optimized carbonate-brine interface reaction parameters. Z0, Z1, Z2 denote charge change at the 0, 1, and 2 planes, respectively. The optimized log-K values are consistent with several literature values[5,30,32,41,52].

No.	Reaction	log-K at:			Z0	Z1	Z2
		25°C	65°C	120°C			
8	$>CaOH^{-0.75} + H^+ <=> >CaOH_2^{+0.25}$	11.8	10.82	9.89	1	0	0
9	$>CaOH^{-0.75} + CO_3^{-2} <=> >CaCO_3^{-1.75} + OH^-$	1.25	1.35	1.5	-0.04	-0.96	0
10	$>CaOH^{-0.75} + SO_4^{-2} <=> >CaSO_4^{-1.75} + OH^-$	2.47	2.86	3.1	0.44	-1.44	0
11	$>CaOH_2^{+0.25} + Cl^- <=> > CaOH_2^{+0.25}$ .....Cl^-	-1.1	-3.35	-5.4	0	0	-1
12	$>CO_3H^{+0.75} <=> >CO_3^{-0.25} + H^+$	-3.54	-3.0	-3.0	-1	0	0
13	$>CO_3H^{+0.75} + Ca^{+2} <=> >CO_3Ca^{+1.75} + H^+$	-2.9	-2.35	-1.3	-1	2	0
14	$>CO_3H^{+0.75} + Mg^{+2} <=> >CO_3Mg^{+1.75} + H^+$	-2.9	-2.15	-1.27	-1	2	0
15	$>CO_3^{-0.25} + Na^+ <=> >CO_3^{-0.25}$ .....Na^+	-1.15	-2.1	-2.7	0	0	1
16	C1, F/m^2	2.8					
17	C2, F/m^2	4.5					

2.2. Implementing CSWF

UTCHEM, a three-dimensional, non-isothermal, multiphase flow simulator developed by the University of Texas at Austin.[71] is used to simulate core flooding experiments carried out on cylindrical rock samples. Assess to UTCHEM was acquired from the University of Texas at Austin in 2009, when it was an open source. One-dimensional numerical models with 30 grid blocks in x-direction were used to simulate CSWF processes that were conducted on core samples in the previous studies. A wettability indicator calculated from ζ-potentials was implemented in the model to account for the effect of CSWF on oil recovery. We achieved this by coupling UTCHEM with PHREEQCRM. PHREEQC, a general-purpose geochemical simulator, is capable of modelling interactions between water and gases, surface complexes, minerals, ion exchangers, and solid solutions[72]. However, coupling PHREEQC with multiphase simulators can be inefficient when running millions of calculations[72]. PHREEQCRM is designed specifically to ease coupling of PHREEQC with multiphase flow simulators. It offers a high-level interface that permits flow simulators to implement geochemical reactions with a minimum amount of programming, whilst ensuring utilisation of the full functionality of PHREEQC's reaction capabilities. Thus, it allows one to use PHREEQC as a reaction engine for the transport simulator [72]. The method utilized to model the CSWF is described below:

a. Coupling UTCHEM with PHREEQCRM

Although, in fluid flow, transport and geochemical reactions occur simultaneously, this work solved transport and reaction equations separately, using UTCHEM for fluid transport and

PHREEQCRM for geochemical reaction calculations. A sequential non-iterative approach reported by Korrani et al.[43,51,73,74] and Parkhurst & Wissmeier.[72] was adopted. Thus, this approach does not require iteration between the two simulators.[43]. In this method, chemical reactions are not involved when UTCHEM solves the mass conservation equation. It is worth mentioning that PHREEQCRM calculated number of moles of mineral and surface species are saved automatically at each time step.[43,75]. Hence, it is only the solution components that are modified at each time step.[43]. The coupling steps are summarized below:

i. UTCHEM calculates elements concentration (mol/l) in brine after each time-step in each numerical grid-block
ii. This data is exported to PHREEQCRM, which simulates the zeta potential at the oil-brine and rock-brine interfaces
iii. Zeta potential is imported into UTCHEM model, which is then used to compute wettability interpolant for relative permeability calculation. Also, PHREEQCRM calculated elements concentrations are imported into UTCHEM to update its brine concentration
iv. With the recalculated relative permeability for each grid-block, the next time step is simulated and produces new ion concentrations
v. The procedure repeats until the final time-step, consistent with the experimental data is reached

Figure 4 below shows the UTCHEM-PHREEQCRM flowchart. It is important to note that total hydrogen, total oxygen, and charge imbalance (CB) are also transported to PHREEQCRM. To obtain equivalent volume of solution (V_{H2O}) in UTCHEM and PHREEQCRM grid-blocks, UTCHEM grid block volume (in litres), water saturation and porosity are used in PHREEQCRM to calculate V_{H2O}. The data transfer (i.e.: reading of data) between UTCHEM and PHREEQCRM occurred in the computer memory, as such, writing and/or reading of files is not required. We verified our coupled UTCHEM-PHREEQCRM model with PHREEQC before using it for the CSWF simulations. Detailed description of the verification process is given in the discussion of results section (section 3.3).

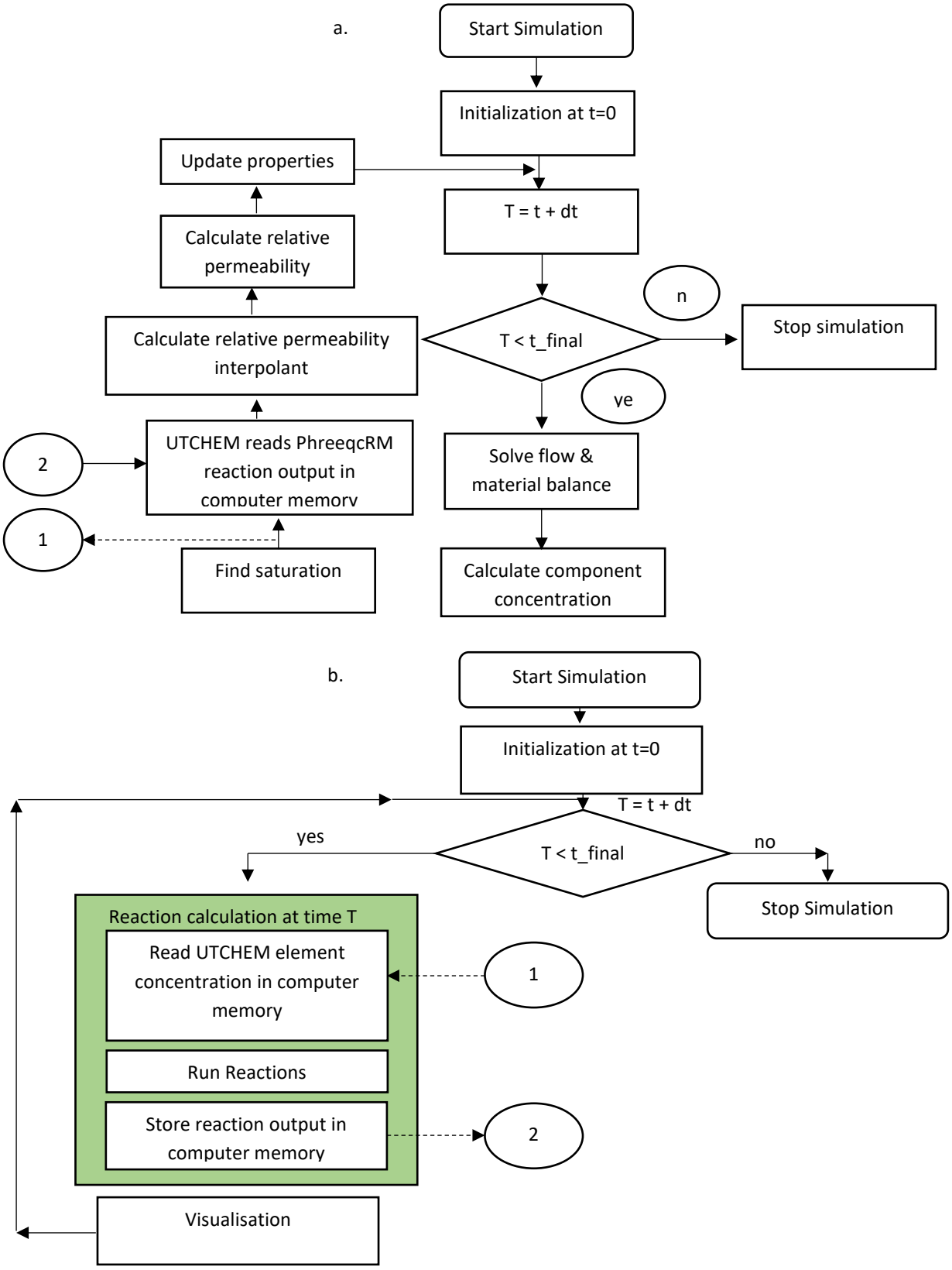

Figure 4: UTCHEM-PHREEQCRM coupling flowchart. (a) UTCHEM simulator, and (b) PHREEQCRM simulator.

b. Implementation of wettability alteration

In our UTCHEM CSWF simulation, we model wettability alteration due to the low salinity effect via a shift in relative permeability curves. Therefore, two sets of relative permeability curves are used; one for the initial conditions of brine salinity and the other, for final state, where the total concentration of the pore-space aqueous phase is reduced to the salinity of the injected low salinity brine. The two relative permeability curves are then interpolated to obtain the relative permeability consistent with the current carbonate-oil-brine (COB) condition. We developed wettability interpolant that considers ζ-potentials at oil-brine and rock-brine interfaces. Several researchers[39–41,76] have pointed out that oil surface species (i.e.: COO^-, $COOCa^+$, NH_2^+, $COOMg^+$) can be adsorbed at the carbonate surface to alter wettability. Nonetheless, it is important to note that a certain amount of work must be done for the adsorption of ionic species in electrostatic models. This electrostatic work done is equivalent to $exp^{\left(\frac{mF\psi}{RT}\right)}$.[57], where F is Faraday constant $\left(96485\ \frac{C}{mol}\right)$; R is universal gas constant $(8.314\ J/K.mol)$; T is absolute temperature in K; ψ is potential in volts and m denotes charge at the surface. Bonto et al[41] indicated that oil species must travel through two electrostatic fields (i.e.: oil-brine interface EDL & rock-brine interface EDL) before arriving at the carbonate surface. They further developed a parameter called available adsorption site (Equations 7 and 8), AAS, from triple layer reactions proposed by Goldberg.[49,77] (Equations 5 and 6):

$$SOH + M^{m+} <=> SO^-\ldots M^{m+} + H^+ \qquad (5)$$

$$K = \frac{[SO^-\ldots M^{m+}][H^+]}{[SOH][M^{m+}]} exp\left(\frac{F(m\psi_1 - \psi_0)}{RT}\right) \qquad (6)$$

Then, AAS for COB:

$$AAS_{Ca} = \frac{[CaOH_2^{+0.333}]}{exp\left(\frac{\psi_{rock}-\psi_{oil}}{T}\right)} \qquad (7)$$

$$AAS_{CO_3} = \frac{[CO_3^{-0.333}]}{exp\left(\frac{\psi_{oil}-\psi_{rock}}{T}\right)} \qquad (8)$$

Where SOH is the mineral surface species, M^{m+} is ion M in brine with charge m, $SO^-\ldots M^{m+}$ is surface adsorbed ion M, ψ_1 is potential at 1-plane, ψ_0 is potential at 0-plane, and K is equilibrium constant for the reaction. Large AAS implies high available $CaOH_2^{+0.333}$ and/or $CO_3^{-0.333}$ sites to adsorb oil, signifying low oil recovery. We adopted this formulation and developed a wettability parameter.

Regarding COB system, SOH and M^{m+} are equivalent to rock-brine and oil-brine surface species, respectively. $SO^-\ldots M^{m+}$ also corresponds to the adsorbed oil species at the rock surface. However, numerous competing reactions occurring between the rock and the oil surface species make it difficult to identify the specific species responsible for wettability alteration[39]. Brady et al[39,40] suggested several of these COB reactions and proposed that the electrostatic linkages of $>CaOH_2^+$ and COO^-, and also $>CO_3^-$ and NH^+ are dominants. They further explained that the presence of Ca^{+2}, Mg^{+2} and SO_4^{-2} ions in brine can affect the electrostatic linkage. That is, SO_4^{-2} adsorption at the carbonate surface can reduce $>CaOH_2^+$

sites whereas Ca^{+2}, Mg^{+2} adsorptions can reduce COO^- sites at the oil surface. Ding et al[76] also attributed adsorption of oil to the interactions between: $>CaOH_2^+$ and COO^-, $>CO_3Ca^+$ and COO^-, $>CO_3Mg^+$ and COO^-. On the other hand, Korrani et al[44] did not observe any correlations between sum product of the surface species and oil recovery as it failed to predict most of the CSWF that they conducted. Nonetheless, oil adhesion does not depend on only surface species but also the electrostatic force (electrostatic work) between the oil and the rock surface, as observed in Equation 7 - 8. That is, irrespective of the surface linkage involved, amount of the adsorbing species relates to the electrostatic force between oil and rock.

We propose a wettability indicator, β, that is related to the total electrostatic work. This count for the total work associated with two planes with ζ-potentials. Therefore, the proposed wettability indicator is calculated from the ζ-potentials at the oil-brine and the rock-brine interfaces, and the value of β gives an indication of the wetting condition of the reservoir. β is calculated as:

$$\begin{cases} \beta = exp\left[\frac{F(|\psi_{ob}|+|\psi_{rb}|)}{RT}\right] \times (-1)^n, & \text{for } (\psi_{ob} \times \psi_{rb}) \neq 0 \\ \beta = 0\,, & \text{for } (\psi_{ob} \times \psi_{rb}) = 0 \end{cases} \qquad (9)$$

where:

n = 2; for $(\psi_{ob} \times \psi_{rb}) > 0$

n = 1; for $(\psi_{ob} \times \psi_{rb}) < 0$

ψ_{ob} and ψ_{rb} are ζ-potentials (in volts, V) at the oil-brine and the rock-brine interfaces, respectively. $(-1)^n$ in Equation 9 simplifies the effect of charge (m) on the total work. A high value of the wettability indicator implies strong electrostatic forces (either attractive or repulsive) between the oil and the rock. The reservoir is classified as an oil-wet system when $\beta < 0$, and this occurs when the ζ-potentials are of the opposite polarities. $\beta > 0$ occurs when both ζ-potentials are of the same polarities, indicating a water-wet reservoir. However, the reservoir is neutral wet or intermediate wet when $\beta = 0$, which happens when one or both ζ-potentials are zero. Therefore, if wettability is controlled by the electrostatic interactions, then only when the electrostatic repulsion (or attraction) between rock-brine and oil-brine interfaces is strong, i.e., both ζ-potentials at rock-brine and oil-brine interfaces are of significant magnitude and same (or opposite) polarities, that the mineral surface will be strongly water-wet (or oil-wet). In CSWF, the objective is to increase β from its initial value to a positively larger value at the final state to improve the oil recovery factor.

To apply the new wettability indicator concept in CSWF simulations, two sets of β are calculated: one for the initial conditions of brine salinity ($\beta^{initial}$) and one for the final state, where the total concentration of the pore-space aqueous phase is reduced to the salinity of the injected CSW (β^{final}). Then, during a time-step, β^t consistent with the current COB condition is calculated. The relative permeability interpolant, ω, is therefore calculated as:

$$\omega = \frac{\beta^t - \beta^{final}}{\beta^{initial} - \beta^{final}} \qquad (10)$$

$$[\,\omega = \max(\omega, 0)\ or\ \omega = min(\omega, 1)]$$

β^t is assumed to not exceed $\beta^{initial}$ or β^{final}, and even at some point in transition, from oil-wet to water-wet where β^t exceeds $\beta^{initial}$ or β^{final}, ω calculated will be zero or one. We then interpolated end-point relative permeabilities and Corey's exponents (Equations 11 – 14):

$$K_{ro}^{o} = \omega K_{ro}^{ow} + (1-\omega)K_{ro}^{ww} \qquad (11)$$

$$K_{rw}^{o} = \omega K_{rw}^{ow} + (1-\omega)K_{rw}^{ww} \qquad (12)$$

$$n_o = \omega n_o^{ow} + (1-\omega)n_o^{ww} \qquad (13)$$

$$n_w = \omega n_w^{ow} + (1-\omega)n_w^{ww} \qquad (14)$$

Reduction in residual oil saturation due to CSWF effect was expressed using Equation 15, similar to interpretation of the end-point relative permeability curves:

$$S_{or} = \omega S_{or}^{ow} + (1-\omega)S_{or}^{ww} \qquad (15)$$

where: K_{ro}^{ww} corresponds to the end-point relative permeability to oil at water-wet condition, K_{ro}^{ow} is end-point relative permeability to oil at oil-wet condition, and K_{ro}^{o} is current end-point relative permeability to oil. K_{rw}^{ww}denotes end-point relative permeability to water at water-wet condition, K_{rw}^{ow} is end-point relative permeability to water at oil-wet state and K_{rw}^{o} is current end-point relative permeability to water. Also, n_o^{ow} is oil Corey's exponent at oil-wet state, n_o^{ww} is oil Corey's exponent at water-wet state and n_o is current Corey's exponent for oil. n_w^{ow} is water Corey's exponent at oil-wet state, n_w^{ww} is water Corey's exponent at water-wet state and n_w is current Corey's exponent for water. S_{or}^{ww} corresponds to residual oil saturation at water-wet state; S_{or}^{ow} is residual oil saturation at oil-wet condition and S_{or} denotes current residual oil saturation.

Finally, relative permeability to water (K_{rw}) and oil (K_{ro}) during CSWF process is calculated from Brooks and Corey's correlation (Equations 16 - 18):

$$K_{rw} = K_{rw}^{o}\,(S_n)^{nw} \qquad (16)$$

$$K_{ro} = K_{ro}^{o}\,(1-S_n)^{no} \qquad (17)$$

$$S_n = \frac{S_w - S_{wc}}{1 - S_{wc} - S_{or}} \qquad (18)$$

where S_w denotes water saturation; S_{wc} is irreducible water saturation; S_n is normalized water saturation.

2.3. CSWF data sets for validation of the model

To investigate the accuracy of the proposed TLM-CSWF model, it was tested against different sets of experimental results that were reported by Fathi et al.[13], Yousef et al.[78], Austad et al.[7], and Sharma & Mohanty[79]. Fathi et al.[13] performed tertiary CSWF experiments

where formation brine (FW) was first injected followed by seawater (SW), and then 10000 times diluted SW (SW/10000). Similarly, Yousef et al.[78] and Austad et al.[7] conducted tertiary CSWF tests. The experimental data from these studies is given by Table 3 and 4, and we used these oil recovery results in the next sections of the study.

Table 3: Properties of rock and oil used by the authors

Property	**Fathi (2010)**	**Yousef (2010)**	**Austad (2012)**	**Sharma & Mohanty (2018)**
Porosity, fraction	0.45	0.25, 0.2465	0.18	0.28
Permeability, mD	1 - 2	39.6, 68.3	1.2	20
Diameter, cm	3.81	3.8, 3.81	3.8	3.81
Length, cm	7.0	16.24, 23.65	8.1	30.48
Initial Water saturation, fraction	0.08	0.104, 0.144	0.07	1.0
Initial Pressure, bar	10	13.8	10	6.89
Reservoir Temperature, ^{o}C	120	100	110	120
Injection rate, cm^3/day	36	1440	144	173.74
AN, mg KOH/g oil	1.9	0.25	0.7	-
BN, mg KOH/g oil	-	-	0.42	-
Oil density, g/cm^3 at 25ºC	0.811	0.72 at 100ºC	0.818 at 20ºC	-
Oil viscosity, cp at 25ºC	3.38	2.03 at 100ºC	3.8 at 20ºC	-
Injection sequence	FW=>SW	FW=>SW=>0.5SW =>0.1SW=>0.05SW	FW=>0.01FW	a. FW=>SW b. FW=>SW=>SW4SO4

Table 4: Composition of the brines used by the authors. For SW_2SO_4^{-2} and SW_4SO_4^{-2}, SO_4^{-2} concentration in the SW is increased by two-fold and four-fold, respectively.

Fathi et al (2010), mol/l								
Brine/ion	**Na^+**	**Ca^{2+}**	**Mg^{2+}**	**SO_4^{-2}**	**Cl^-**	**K^+**	**HCO_3^-**	**TDS**
FW	1.0	0.029	0.008	0.0	1.07	0.005	0.009	62800 (ppm)
SW	0.45	0.013	0.045	0.024	0.525	0.01	0.002	33390 (ppm)
Yousef (2010), ppm								
FW	59491	19040	2349	350	132060	0	354	213734 (ppm)
SW	18300	650	2110	4290	32200	0	120	57670 (ppm)
Austad (2012), mol/l								
FW	2.62	0.437	0.076	0	3.643	0	3e-3	208940 (ppm)
FW/100	262e-2	4.37e-3	7.6e-4	0	3.643e-2	0	3e-5	2089.4 (ppm)
Sharma & Mohanty (2018), ppm								
FW	41411	11686	2763	215	103002	0	0	149160 (ppm)
SW	12891	510	1600	3485	26578	0	0	41127 (ppm)

3. Results and Discussion

3.1. oil-brine interface ζ-potential

Before using the proposed TLM model for CSW simulations, we validated it with experimentally measured ζ-potentials from past studies. It should be noted that matching our model to experimental ζ-potential data was performed with PHREEQC software. To test the model reliability, different cases of experimental data were used (i.e., experiments with different oil and brine properties). Experimentally, oil-brine ζ-potential is measured by Electrokinetics using oil-water emulsions. For simplification, single-stage equilibration and two-stage equilibration were used to describe the experimental condition at which ζ-potential was measured. Single-stage equilibration denotes the state whereby ζ-potential is measured after initial equilibration of the oil-brine emulsion without modifying its pH, salinity, or composition. Two-stage equilibration represents the state whereby ζ-potential is measured after the initial equilibrated emulsion is modified. Thus, either pH of the equilibrated emulsions is altered (by addition of HCl/NaOH) or addition of specific brine(s). It is worth noting that whichever method was involved in the measurement, the same approach was followed in the modelling. Furthermore, we compared the ζ-potentials from our TLM with outputs from the existing oil-brine SCM.

3.1.1. Comparing the oil-brine TLM with experimental cases

In this part, ζ-potentials of the oil-brine interface from four experimental cases were compared with the proposed TLM in this study, which is explained below:

Case 1:

We first present results of the model matched to the experimental results of Alshakhs & Kovscek.[9] (Figure 5). They measured oil-brine ζ-potential at 25°C (brine composed of Na, Cl, Mg, SO_4). Measurement was undertaken at two-stage equilibration state, by modifying pH of the initial equilibrated oil-brine emulsion solution. We calculated acid site-density of 12.35 sites/nm^2 and base site-density of 13.4 sites/nm^2 from the TAN (1.15 mgKOH/g oil) and TBN (1.25 mgKOH/g oil), respectively. We also used our earlier calculated capacitances (C1 = 2.84, C2 = 4.48 F/m^2). Hence, the only parameter that we tuned in matching the model to the experimental data was oil-brine interface reactions constants. The optimized reactions constants are provided in Table 1.

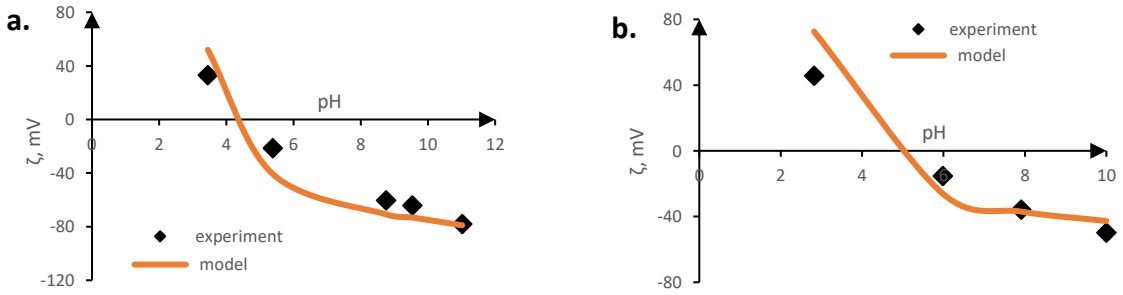

Figure 5: comparison of the model (this study) and experimental data (Alshakhs & Kovscek.[9]) of oil-brine ζ-potential. (a) 1000 times diluted sea water, and (b) 100 times diluted $MgSO_4$

Case 2:

The oil-brine interface model validation was extended to the experimental ζ-potential data of Buckley et al.[11] (Figure 6). They measured ζ-potential using NaCl brines of different concentrations (i.e.: 0.1, 0.01, 0.001M) and two different oils (Moutray and Leduc oil) at 25°C. They used two-stage equilibration process by modifying pH of the equilibrated emulsion solution. Also, we used our capacitance values (C1 = 2.84 and C2 = 4.48 F/m^2) and the optimized oil-brine reactions constants generated from the previous match (i.e.: Alshakhs & Kovscek.[9] matched equilibrium constants). The authors reported TAN of 0.26 mgKOH/g oil and 0.15 mg KOH/g for Moutray and Ludec oil, respectively. However, TBN was not given. Therefore, we directly used the reported acid site-density of 0.5/nm^2 and 1.55/nm^2 for Moutray and Leduc oil, respectively. Also, we used the reported base site-density of 0.1/nm^2 and 1.4/nm^2 for Moutray and Leduc oil, respectively. The model matches well with the experimental data. ζ-potential of both oils remained positive until the iso-electric point (IEP), where it begins to shift towards negative. The ζ-potential increasingly becomes negative with increasing pH because the acidic oil component greatly dissociates at high pH value, generating more negative charges at the oil-brine interface. It can be observed that magnitude of the ζ-potential decreases with increasing NaCl concentration whiles polarity remained unchanged. As we mentioned earlier, increasing ionic strength decreases ζ-potential.

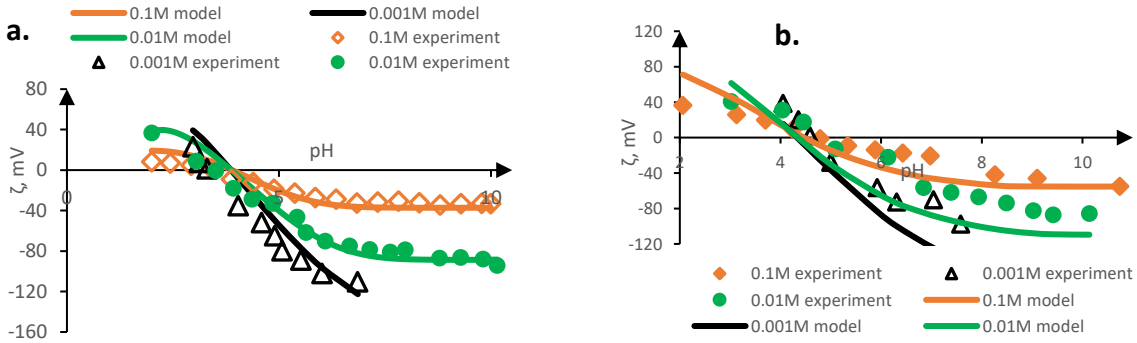

Figure 6: comparison of the model (this study) and experimental data (Buckley et al.[11]) of oil-brine ζ-potential with various concentrations of NaCl brine. (a) Moutray oil, and (b) Leduc oil

Case 3:

We also matched our oil-brine interface model to experimental ζ-potential results of Lu et al[80]. They measured oil-brine ζ-potential using two different brines (NaCl and $MgCl_2$) of varying concentrations. The experiment was conducted under single-stage equilibration process at 25°C. Again, we used the same oil-brine reactions constants optimized earlier and our calculated capacitance values. We obtained acid site-density (1.93 sites/nm^2) and base site-density (12.2 sites/nm^2) calculated from the reported TAN (0.18 mgKOH/g oil) and TBN (1.14 mgKOH/g oil), respectively. The model predicted accurately the ζ-potential trend (Figure 7).

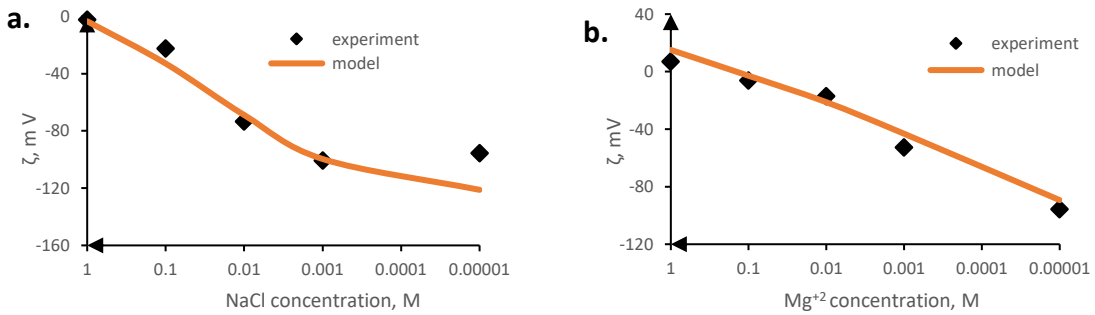

Figure 7: comparison of the model (this study) and experimental data (Lu et al.[80]) oil-brine ζ-potential with various concentrations of NaCl and $MgCl_2$ brines. (a) NaCl brines, and (b) $MgCl_2$ brines

Case 4:

Our next match is Chow & Takamura.[81] oil-brine ζ-potential data measured at 25°C. Two separate brines: NaCl brine of different concentrations, and NaCl-$CaCl_2$ mixture were used. Also, two oil types (bitumen and Moutray oil) were used for the experiment. The authors reported only TAN (0.26 mgKOH/g oil) for the Moutray oil and TAN (2.0 mgKOH/g oil) for the bitumen. We calculated bitumen acid site-density (21.5 sites/nm^2) and Moutray oil acid site-density (2.79 mgKOH/g oil) from their TAN. We therefore matched the ζ-potential data to our model by using the base sites-densities as tuning parameter. Capacitances and all other oil-brine reactions constants remained unchanged. The model results are shown by Figure 8. Base site-densities were estimated as 0.35 site/nm^2 for bitumen, and 0.27 site/nm^2 for Moutray oil. Some of the model results could not match the experimental data, and this could be caused by the base site-densities used in the model.

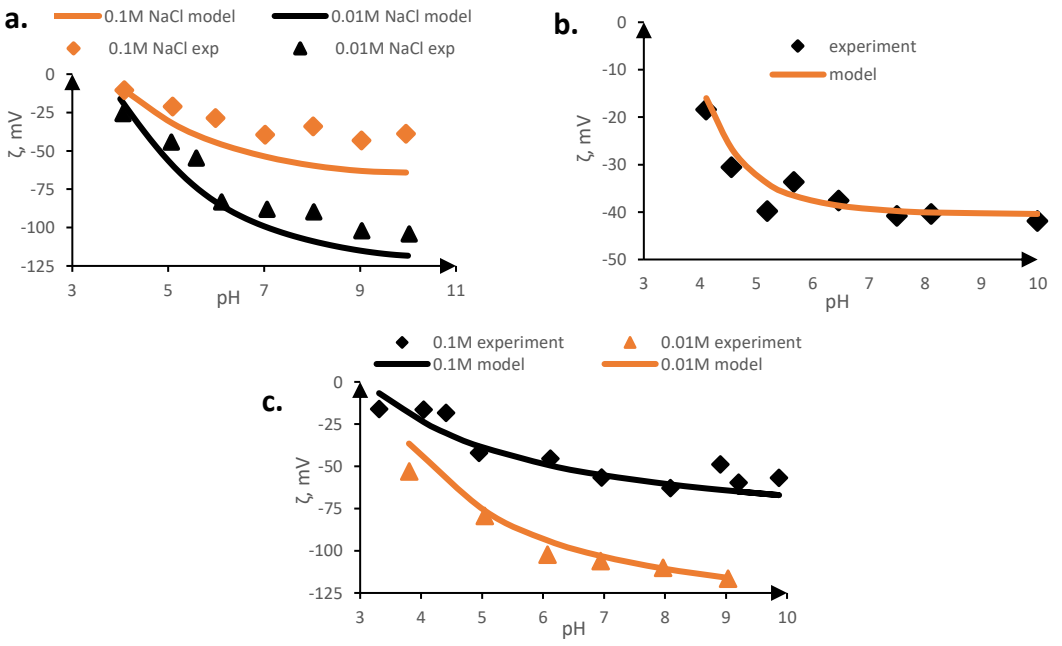

Figure 8: comparison of the model (this study) and experimental data (Chow & Takamura.[81]) of oil-brine ζ-potential with two different oils and various brines. (a) Moutray oil and NaCl brine, (b) Moutray oil and NaCl-$CaCl_2$ mixture, and (c) bitumen and NaCl brine.

3.1.2. Comparing the oil-brine TLM with DLM

We now employed existing oil-brine SCM to simulate some experimental ζ-potential data sets. Brady et al.[40,41] proposed DLM for oil-brine interface interactions (Table 5). However, their model was not matched with experimental ζ-potential data because the authors were more interested in surface species, which were used in bond product estimation. We used their model parameters and also our TLM to calculate experimental ζ-potential of Buckley et al.[11]. We do not intend to compare the two models but to demonstrate that TLM calculated potentials can be used directly as ζ-potential, without the need to employ any correlations for their estimation. It should be pointed out that the NaCl solution used for the experiment is a symmetrical electrolyte solution. Moreover, some of the DLM potentials exceeded 25mV, hence, Gouy-Chapmann relation (Equation 19).[53,64] was used to estimate ζ-potential from the DLM surface potential:

$$\zeta = \psi_x = \frac{4k_b}{e}\gamma \exp(-Kx) \qquad (19)$$

$$\gamma = tanh\left(\frac{e\psi_o}{4k_bT}\right) \qquad (20)$$

$$\frac{1}{K} = \left(\frac{\varepsilon_r\varepsilon_0 k_b T}{2N_A e^2 I}\right)^{0.5} \qquad (21)$$

where: I = ionic strength (mol/m^3), ε_0 = permittivity of free space ($8.854 \times 10^{-12}\ C^2/J.m$), ε_r = relative permittivity of water (78.5 at 25^{o}C), k_b = Boltzmann constant. Also, T = absolute temperature (K), N_A = Avogadro number ($6.02 \times 10^{23}\ mol^{-1}$), e = elementary charge ($1.602 \times 10^{-19} C$), $\frac{1}{K}$ = Debye length (m), x = slip plane distance (m), ψ_o = surface potential (Volts), and ζ = zeta potential (Volts). To compute DLM ζ-potential, we assumed that $x = 0.6nm$.[11]. The result shows that both the TLM and DLM produced good match with the experimental ζ-potential data for the 0.1M NaCl solution (Figure 9). The TLM, however, offered a better match for the 0.01M NaCl solution. As we have indicated earlier, DLM ζ-potential computation from surface potential involving asymmetrical solution would require complex equation.[53]. CSWF, usually, involves asymmetrical solution, which implies that complex correlation is required to estimate zeta potential from the DLM calculated surface potential. As such, TLM, which estimates ζ-potential directly without the need to introduce any correlation is suggested.

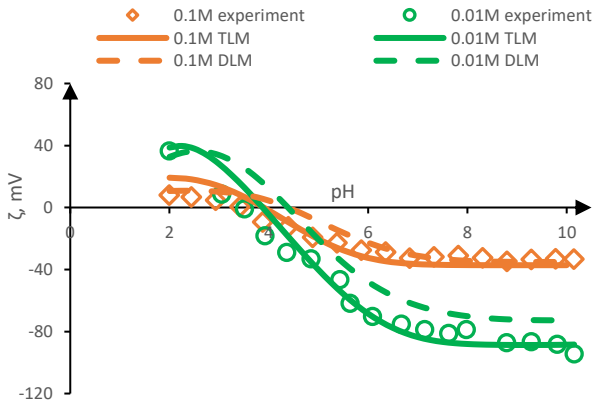

Figure 9: comparison of oil-brine interface potential calculated with our model (TLM) and DLM proposed by Brady et al[40,41]. Buckley et al experimentally measured ζ-potential was used for the modelling.[11].

Table 5: Brady et al proposed DLM [39,40,70]

No.	Reaction	log-K at 25°C
1.1	>RCOOH <=> >RCOO$^-$ + H$^+$	-5.0
2.1	>NH+ <=> >N + H$^+$	-6.0
3.1	>RCOOH + Ca^{+2} <=> >RCOOCa$^+$ + H$^+$	-3.8
4.1	>RCOOH + Mg^{+2} <=> >RCOOMg$^+$ + H$^+$	-4.0

3.1.3 Comparing the oil-brine TLM with existing TLMs

Another existing oil-brine SCM compared with our TLM is Takeya et al.[37] proposed TLM. The authors measured oil-brine interface ζ-potential at 50°C using various brine, and also modelled their experimental data with a TLM. However, they did not consider Na^+ adsorption and >NH reactions in their model. On matching our TLM to the experimental ζ-potential data, three scenarios were simulated: (a) both >NH and Na^+ surface reactions considered in the model, (b) only >NH surface reactions omitted from the model, and (c) only Na^+ surface reaction omitted from the model. We calculated acid site-density (4.19 sites/nm^2) from the reported TAN (0.39 mgKOH/g oil), and base site-density (20 sites/nm^2) from the TBN (1.86 mgKOH/g oil). Takeya et al.[37] did not report brines and emulsion pH, hence, we assumed brines pH of 7.0. Using our calculated capacitance values (C1 = 2.84; C2 = 4.48 F/m^2), new oil-brine reactions constants were optimized (as this experiment was conducted at 50°C) by matching the model to Takeya et al.[37] data sets. The optimized equilibrium constants are given in Table 6 .

Table 6: oil-brine reaction constants at 50°C.

No.	Reaction	log-K at 50°C
1	>RCOOH <=> >RCOO$^-$ + H$^+$	-4.5
2	>NH+ <=> >N + H$^+$	3.5
3	>RCOOH + Na$^+$ <=> >RCOONa + H$^+$	-4.52
4	>RCOOH + Ca^{+2} <=> >RCOOCa$^+$ + H$^+$	-3.63
5	>RCOOH + Mg^{+2} <=> >RCOOMg$^+$ + H$^+$	-3.2

It can be observed that omitting Na^+ ion surface reaction from the model did not have any impact on the ζ-potential results (Figures 10 and 11). On the other hand, >NH omission significantly affected the model ζ-potential results.

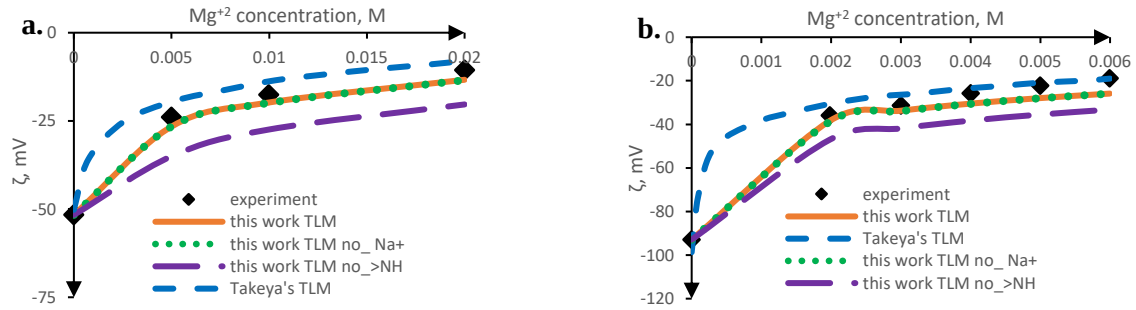

Figure 10: comparison of our oil-brine TLM to Takeya et al.[37] TLM. (a) measured ζ-potential at constant pH of 7, and (b) measured ζ-potential at constant ionic strength of 20mM. "TLM_no Na+" denotes the model calculation where Na+ ion adsorption is omitted from the oil-brine interface reaction calculations. Likewise, "TLM_no >NH" is for >NH omission.

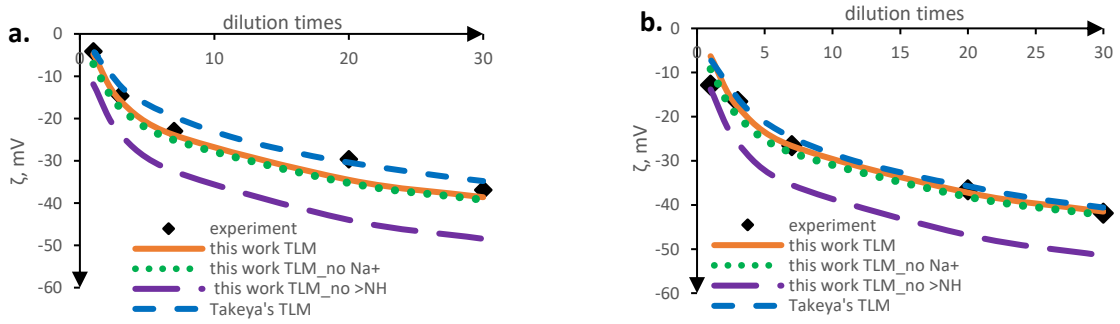

Figure 11: comparison of our oil-brine TLM to Takeya et al.[37] TLM. (a) seawater measured ζ-potential, and (b) formation water ζ-potential. "TLM_no Na^+" denotes the model calculation where Na^+ ion adsorption is omitted from the oil-brine interface reaction calculations. Likewise, "TLM_no >NH" is for >NH omission.

We further investigated this observation by calculating the oil-brine interface reactions at 25°C. This time, we used our 25°C oil-brine reactions constants while maintaining all other parameters (i.e.: acid and base sites-densities; capacitances, brine properties). It should be noted that we compare only our model results since Takeya et al.[37] did not perform experiments at 25°C. It can be identified from Figure 12 that removal of both Na^+ and >NH surface reactions reduced the calculated ζ-potential at 25°C, although, the magnitude is brine-related. Moreover, the impact of >NH surface reaction is greater than the effect of Na^+. At 50°C, kinetic energy of the species increases and the divalent ions having higher affinity to the surface, more of these ions reach the oil surface than Na^+. Therefore, the obtained results for Na^+ surface reaction at 25°C and 50°C can be related to temperature as removing Na^+ surface reactions at 50°C did not affect ζ-potential. Other influencing factor can be the dissociation of the carboxylic group with temperature.

Figure 12: effects of >NH and Na+ surface reactions on oil-brine ζ-potential at 25°C.

The BN/AN ratio of the Takeya et al.[37] experimental oil is approximately 5.0, and we thought this might have contributed to the observed >NH ζ-potential results. We therefore employed Alshakhs & Kovscek[9] experimental data we earlier matched our model to (Figure 5). This oil has BN/AN ratio of approximately 1.0, and we performed this calculation at 50°C and 25°C. It should be noted that we compare only our model results. We observed that omitting the Na^+ surface reaction did not have any impact on the oil-brine interface ζ-potential at both 50°C and 25°C, whereas >NH omission produced more negative ζ-potential (Figure 13a). This suggests that the observed >NH trend might not be related to BN/AN ratio. To confirm this, we used Alshakhs & Kovscek[9] SW/1000 brine and Takeya et al.[37] oil properties, and calculated ζ-potential at 50°C and 25°C. Again, similar trend was observed (Figure 13b). Another ζ-potential data was computed from Takeya et al.[37] SW and Alshakhs & Kovscek[9] oil. This calculation was performed to study the relationship between ionic strength, brine composition and Na^+ surface reactions. Unlike Alshakhs & Kovscek[9] SW/1000 brine which is devoid of Ca^{+2} and K^+, Takeya et al.[37] SW contains these ions. Also, ionic strength of Alshakhs & Kovscek[9] SW/1000 brine is 1.05 mM, whereas ionic strength of Takeya et al.[37] SW is 0.782 M. We have already indicated that using the Alshakhs & Kovscek[9] SW/1000 brine with Takeya et al.[37] oil or Alshakhs & Kovscek[9] oil, Na^+ surface reaction did not contribute to ζ-potential. However, removal of Na^+ surface reaction reduced the calculated ζ-potential from Takeya et al.[37] SW and Alshakhs & Kovscek[9] oil (Figure 13c).

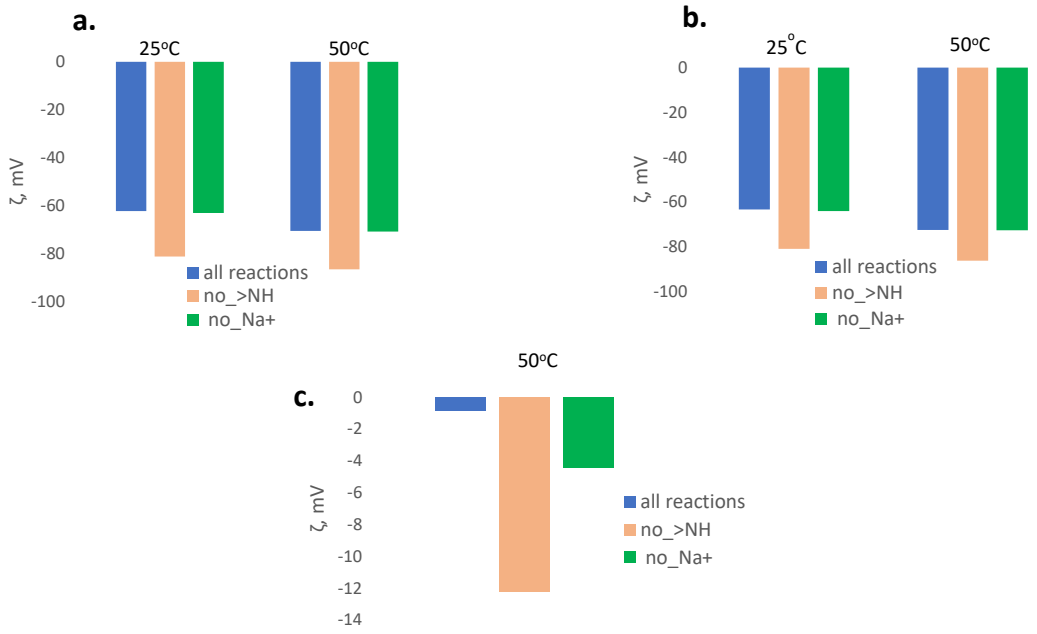

Figure 13: effects of Na^+ and >NH surface reactions on oil-brine ζ-potential at different temperatures, oil and brine composition. (a) calculations from Alshakhs & Kovscek[9] SW/1000 brine and oil properties; (b) calculations from Alshakhs & Kovscek[9] SW/1000 brine and Takeya et al.[37] oil properties; (c) calculations from Takeya et al.[37] SW and Alshakhs & Kovscek[9] oil properties.

It can be proposed from the model results that >NH group significantly impacts oil-brine interface ζ-potential irrespective of temperature, brine composition, and ionic strength. On the other hand, Na^+ ion in brine may influence oil-brine ζ-potential, and this relates to temperature, brine composition, and ionic strength. Therefore, Takeya et al.[37] TLM being able to predict the experimental ζ-potential data could be related to the small acid site-density used by the authors. That is, they used acid site-density of 0.47sites/nm^2, which we obtained 4.19sites/nm^2 when calculated from the TAN. This implies reduced available carboxylic acid (>COOH group) which would dissociate to produce negative ζ-potential values. Based on the above discussion, we suggest that >NH group and Na^+ ion surface reactions can be included in oil-brine SCM as they can impact the calculated oil-brine ζ-potential.

3.2. Carbonate-brine interface ζ-potential

Like the oil-brine interface TLM, the carbonate-brine interface TLM was validated by matching the model to different cases of rock-brine experimental ζ-potential data. Moreover, the carbonate-brine TLM was compared with existing SCM.

3.2.1. Comparing of rock-brine TLM with experimental cases

In this part, ζ-potentials of the rock-brine interface from three experimental cases were compared with the proposed TLM in this study, which is explained below:

Case 1:

We validated our carbonate-brine interactions model with experimental ζ-potential results reported by Awolayo et al.[82] (Figure 14). In their experiment, the initial equilibrium state of formation brine (FW) in contact with carbonate mineral was modified by adding seawater brines (i.e.: SW, $SW0.5SO_4$, $SW2SO_4$, $SW4SO_4$). The numbers in the brines denote

concentration of SO_4 in the specific brine. For instance, $SW2SO_4$ signifies SW with twice SO_4 concentration. As we have indicated in the model description, we used 4.95 site/nm^2 for both calcium and carbonate sites. Moreover, we used C1 = 2.84 and C2 = 4.48 F/m^2. The rock-brine interface reactions constants were then optimized in matching the model to the experimental ζ-potential data. The equilibrium constant generated from our model match is given in Table 2 (i.e.: 25^{o}C constants).

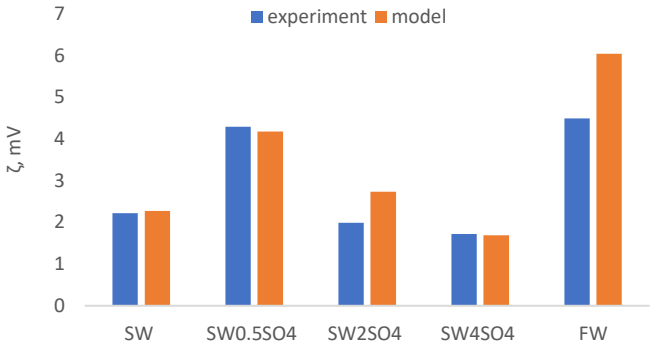

Figure 14: comparison of the model (this study) and experimental data (Awolayo et al.[82]) of rock-brine ζ-potential.

Case 2:

Our next match is ζ-potential results of Al Mahrouqi et al.[29] (Figure 15-17). The authors measured ζ-potential of Estaillades rock with $CaCl_2$, $MgCl_2$ or $NaCl_2$ brines. The optimized equilibrium constants we obtained from simulating Awolayo et al.[82] experimental data was used to model Al Mahrouqi et al.[29] experimental results. Also, same values of site-density and capacitances were used.

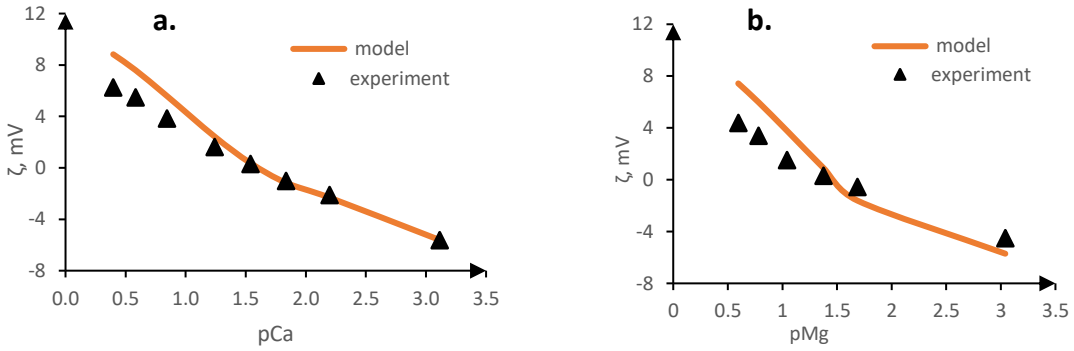

Figure 15: comparison of the model (this study) and experimental data (Al Mahrouqi et al.[29]) of rock-brine ζ-potential with various $CaCl_2$ and $MgCl_2$ brines. (a) $CaCl_2$, and (b) $MgCl_2$. Base electrolyte is 0.5M NaCl brine.

The authors indicated that initial equilibration of the carbonate rock with the NaCl brines produced approximately pH and pCa (i.e.: -log [Ca^{+2}]) of 8.3 and 3.1 $\pm$ 0.1, respectively. The

modelling results also produced approximately pH of 8.33 and pCa = 3.1 ± 0.1, after the initial equilibration with the NaCl brines.

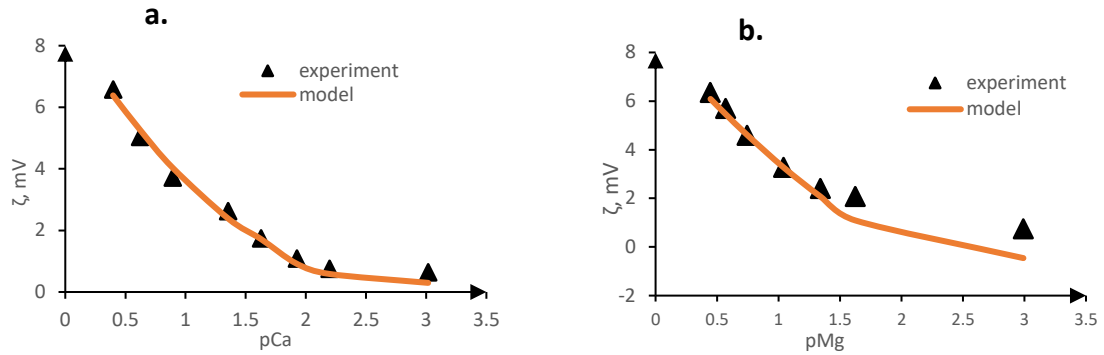

Figure 16: comparison of the model (this study) and experimental data (Al Mahrouqi et al.[29]) of rock-brine ζ-potential. (a) $CaCl_2$, and (b) $MgCl_2$. Base electrolyte is 2.0M NaCl brine.

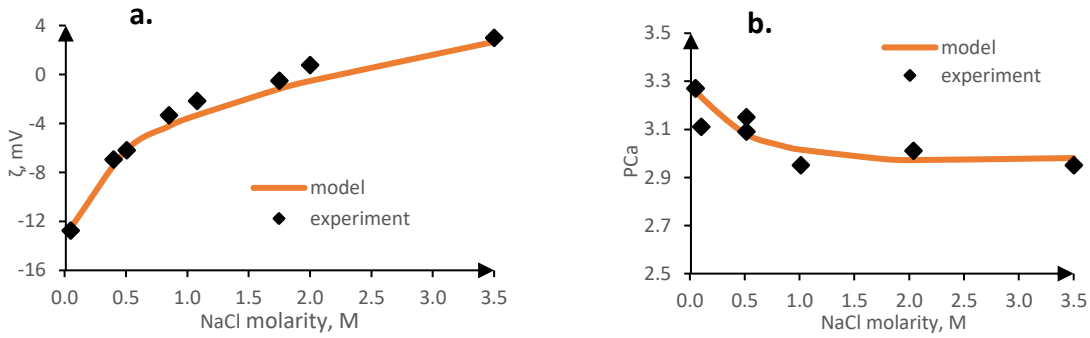

Figure 17: comparison of the model (this study) and experimental data (Al Mahrouqi et al.[29]) of rock-brine ζ-potential with various NaCl concentrations. (a) ζ-potential, and (b) equilibrium pCa during the rock-NaCl brines equilibration process.

Case 3:

Figure 18 shows our model provides a good match with Lu et al.[80] carbonate-brine interface ζ-potential data measured at 25°C and 65°C. Here also, we used C1 = 2.84 F/m^2, C2 = 4.84 F/m^2 and site-density = 4.95 sites/nm^2 for each site. Regarding the 25°C temperature, we used our optimized rock-brine equilibrium constants generated from the previous match (Awolayo et al.[82] matched equilibrium constants), while new equilibrium constants were optimized for the 65°C (Table 7) by matching the model to Lu et al.[80] 65°C experimental data.

Table 7: rock-brine reaction constants at 65C.

No.	Reaction	log-K at 60°C
6	$>CaOH^{-0.75} + H^+ <=> >CaOH_2^{+0.25}$	10.82
7	$>CaOH^{-0.75} + CO_3^{-2} <=> >CaCO_3^{-1.75} + OH^-$	1.35
8	$>CaOH^{-0.75} + SO_4^{-2} <=> >CaSO_4^{-1.75} + OH^-$	2.86
9	$>CaOH_2^{+0.25} + Cl^- <=> > CaOH_2^{+0.25}.....Cl^-$	-3.35
10	$>CO_3H^{+0.75} <=> >CO_3^{-0.25} + H^+$	-3.0

11	$>CO_3H^{+0.75} + Ca^{+2} <=> >CO_3Ca^{+1.75} + H^+$	-2.35
12	$>CO_3H^{+0.75} + Mg^{+2} <=> >CO_3Mg^{+1.75} + H^+$	-2.15
13	$>CO_3^{-0.25} + Na^+ <=> >CO_3^{-0.25} \cdots\cdots Na^+$	-2.1

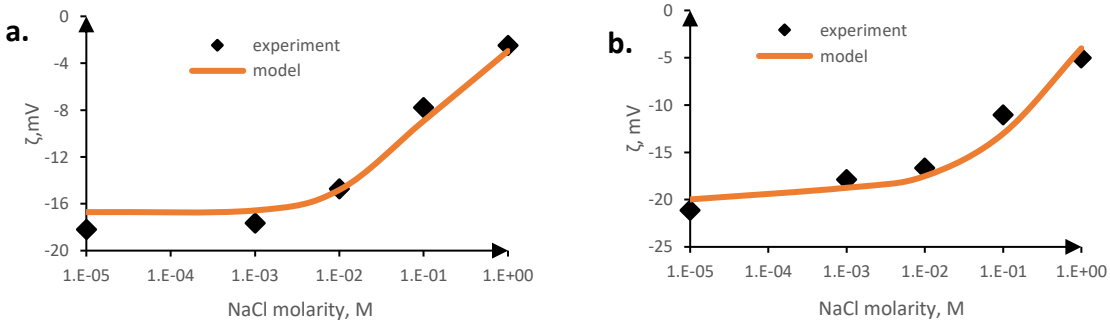

Figure 18: comparison of the model (this study) and experimental data (Lu et al.[80]) of rock-brine interface ζ-potential with various NaCl concentrations. (a) 25°C measured ζ-potential; (b) 65°C ζ-potential measured

3.2.2. Comparing the rock-brine TLM with DLM

Finally, we compared our proposed TLM with the DLM developed by Brady et al.[40]. ζ-potential was estimated from the DLM surface potential using the Gouy-Chapmann relation (equation 20) (Israelachvili.[53]). The result shows that the TLM calculated ζ-potential matches the experimental data better than the DLM ζ-potential (Figure 19). As we indicated in the oil-brine TLM versus DLM model, TLM estimates ζ-potential directly, therefore, no need to introduce any correlation. The experimental results of Al Mahrouqi et al.[29] was used for the simulation. We did not compare our TLM with the few available carbonate-brine TLM because the assumptions and parameters used in those models do not differ much from this work. Hence, we do not expect much difference in the simulation results.

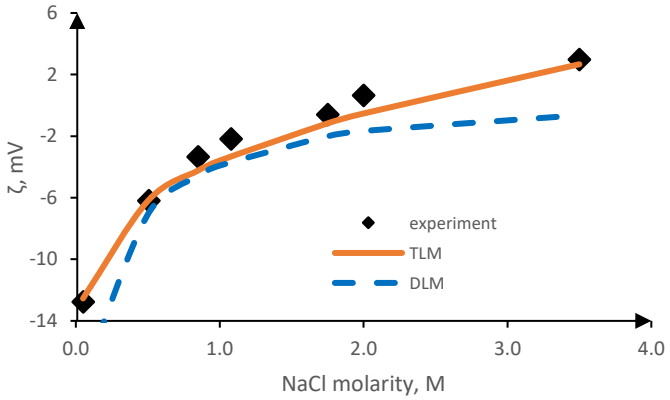

Figure 19: results of rock-brine ζ-potential calculated with our TLM and DLM proposed by Brady et al.[40]

3.3. UTCHEM-PHREEQCRM model validation with PHREEQC

We validated our coupled UTCHEM-PHREEQCRM model using example 11 supplied with the PHREEQC software package[75,83]. The problem consists of a column containing sodium-potassium-nitrate solution in equilibrium with exchanger. The column, having 40 cells (grid size, $\Delta x = 0.002$m), is then flushed with $CaCl_2$ solution and effluent ions concentrations were retrieved. We simulated both the dispersion-free and advective-dispersive transport data with

our model and PHREEQC software, and matched PHRREQC effluent ions with our model (Figure 20). The advective-dispersive case has Peclet number, Pe of 40 and dispersivity, α_L of 0.002m. It should be noted that numerical dispersion in PHRREQC is negligible when $\Delta x \leq \alpha_L$ (Parkhurst & Appelo.[75]). Therefore, to obtain identical Pe between UTCHEM and PHRREQC, we adopted Equation 23 reported by Korrani et al[43,84]:

$$\left(\frac{N\Delta_x}{\alpha_{physical}+\frac{\Delta_x}{2}}\right)_{UTCHEM\_PHREEQCRM} = \left(\frac{N\Delta_x}{\alpha_{physical}}\right)_{PHREEQC} \quad (24)$$

N = total number of cells.

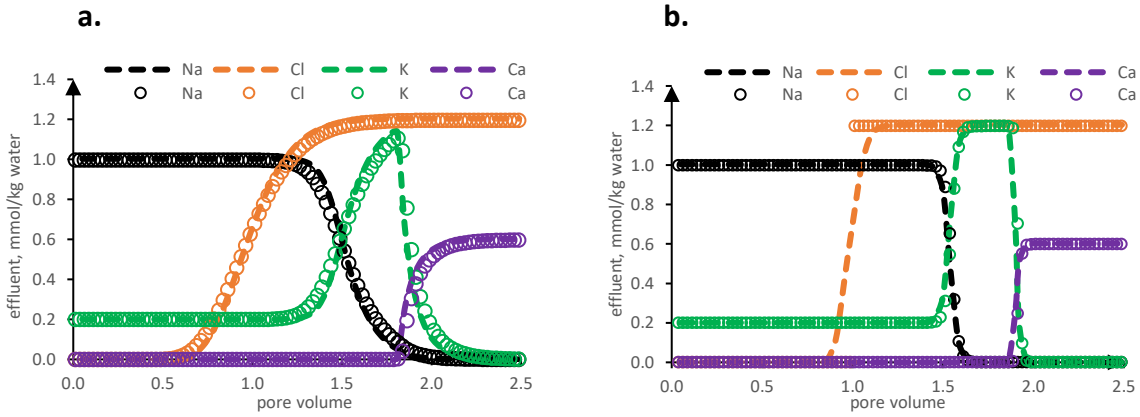

Figure 20: UTCHEM-PHREEQCRM validation with PHREEQC example 11 (Parkhurst & Appelo[75,83]). (a) advective-dispersive results; (b) advective results. Markers denote PHRREQC results and dashes are UTCHEM-PHREEQCRM results.

3.4. UTCHEM-PHREEQCRM model validation with experimental CSWF data

This section presents the simulation results of our UTCHEM-PHREEQCRM model matched with the experimental CSWF data sets. Relative permeability curves are usually measured in the laboratory at the end-point wettability states. However, the CSWF experiments that are simulated in this study did not report relative permeability and capillary pressure curves. Therefore, relative permeability curves at the end points were estimated from the best fit to the experimental oil recoveries. In other word, relative permeabilities were tuned to match the model calculated oil recoveries to the experimental oil recoveries. Capillary pressure was also assumed to be zero in order to reduce the number of tuning parameters.

3.4.1. Modelling of Fathi et al.[13] CSWF experiment

The proposed model was used to simulate core flooding results of Fathi et al[13] (Figure 21). They performed tertiary CSWF by injecting FW at secondary stage and SW at tertiary stage. Secondary injection of FW recovered 56% of original oil in place (OOIP) and was increased to 63% following the SW injection. Like our previous matches, we used same capacitances, rock site-densities, but calculated the oil acid site-density (20.4/nm^2). Fathi et al[13] did not report TBN, hence, we assumed a base site-density of 20.4/nm^2, which is equivalent to the acid site-density. Therefore, relative permeability parameters (end-point relative permeability and Corey's exponents) were optimized to match the model to the oil recovery. The optimized relative permeabilities used to predict the results are shown by Table 8.

Table 8: relative permeability parameters used to simulate Fathi et al[13]experiment

parameter	Initial value	Final value
Swc	0.08	0.08
Sor	0.4	0.34
Krow	0.5	0.5
Krw	0.2	0.2
nw	2	3
no	3	2.5

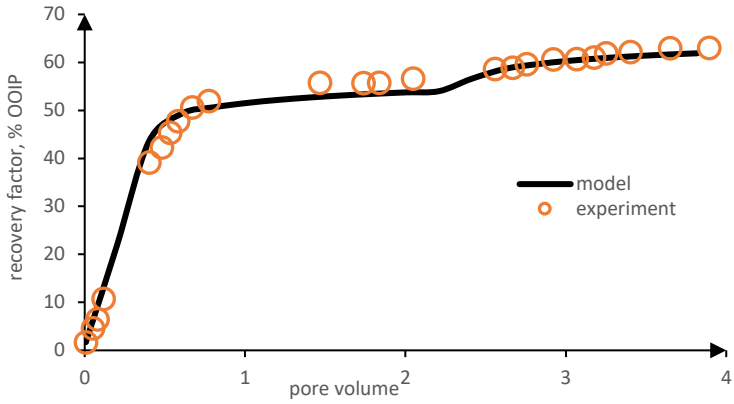

Figure 21: comparison of model (this study) to experimental data (Fathi et al[13]) of oil recovery data

The model calculated wettability indicator shows a shift in the wettability indicator value on switching the injection brine from FW to SW (Figure 22). That is, FW injection produced wettability indicator of -4.37, while switching the injection brine to SW increased the value to 3.39. This implies increased electrostatic repulsive force between the oil and the rock surface, and thus, decreased oil adhesion. Consequently, a shift in the wettability from oil-wet towards water-wet behavior is obtained. There is further reduction in residual oil saturation (Sor) following SW injection. It can be suggested from the magnitude of the wettability indicator that wettability was shifted from weakly oil-wet to weakly water-wet.

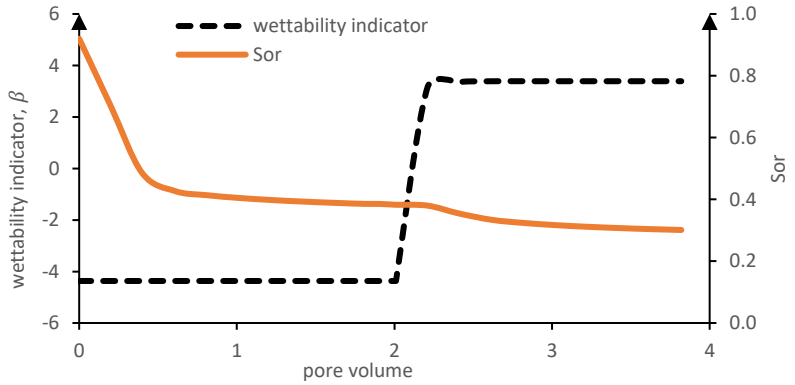

Figure 22: relationship between wettability indicator and residual oil saturation for the brine injections. FW injection produced wettability indicator of about -4.37. During this period, 56% of OOIP was recovered. Switching the injection brine to SW generated wettability indicator of about 3.39. Accordingly, additional 7% OOIP was produced.

ζ-potential of the rock-brine (Figure 23a) and the oil-brine (Figure 23b) interface shows that the two interfaces have opposite ζ-potential during the FW injection. Nonetheless, switching

the injection brine to SW shifted the oil-brine ζ-potential towards positive, although, it remained within negative values. It should be noted that concentration of Mg^{+2} ion in the SW is about six times the Mg^{+2} concentration in the FW. This increased the Mg^{+2} ions in the brine, shifting the reaction: >RCOOH + Mg^{+2} <=> >RCOOMg^{+} + H^{+} to right. The adsorbed Mg^{+2} species at the oil-brine interface is then increased, and the oil-brine ζ-potential is thus, shifted towards positive (Figure 23b). At the same time, the rock-brine ζ-potential shifted to negative values. Unlike the FW, the injected SW contains SO_4^{-2} ion and some past papers argue that adsorption of SO_4^{-2} shifts carbonate ζ-potential to negative values[16,82,85]. It can be suggested that SO_4^{-2}-rich brine with high Mg^{+2} content may sometimes be detrimental to CSWF depending on its generated oil-brine ζ-potential.

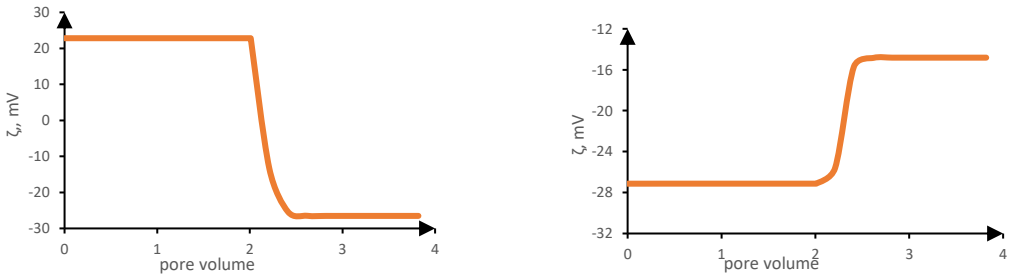

Figure 23: calculated ζ-potential for COB system. (a) rock-brine ζ-potential, and (b) oil-brine ζ-potential.

3.4.2. Modelling of Yousef et al.[78] CSWF experiments

Yousef and co-workers conducted tertiary CSWF with limestone using series of diluted sea water. The carbonate rock was reported to compose of calcite, dolomite and anhydrite (Yousef et al[86]). The authors injected SW at secondary stage, followed by successive injections of two-diluted SW (SW/2); ten-diluted SW (SW/10); twenty-diluted SW (SW/20); hundred-diluted SW (SW/100). The SW/100, however, did not recover additional oil. We simulated their oil recovery with our model and the result is shown by Figure 24.

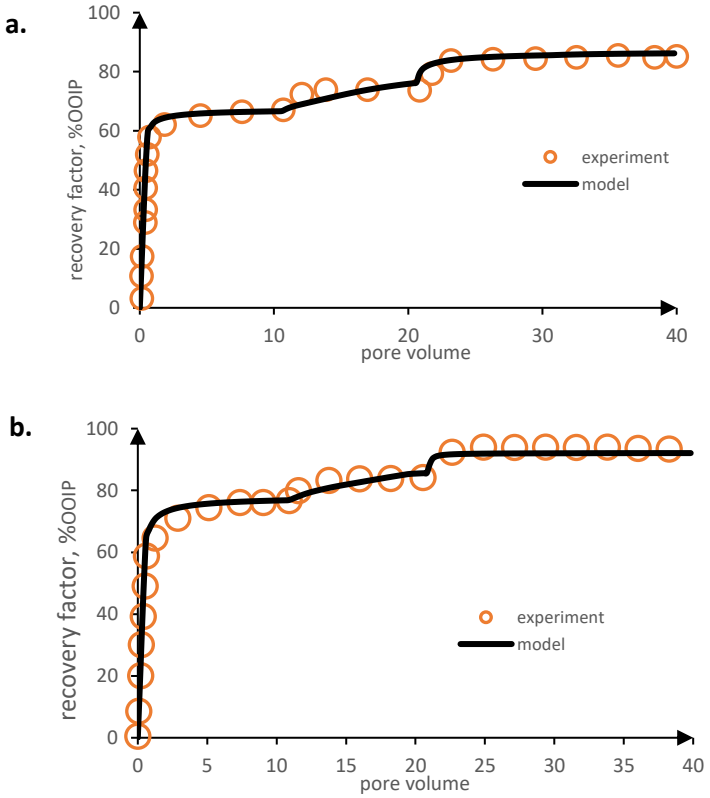

Figure 24: history match of model (this study) to Yousef et al[78] oil recovery data. (a) first Core flood match, and (b) second core flood match.

We calculated acid site-density of 2.69/nm^2 form the TAN (0.25 mgKOH/g oil) and assumed same for base site-density since TBN was not reported. Using our capacitances and carbonate site-density values, relative permeability was optimized to match the model to the experimental oil recoveries. The optimized relative permeabilities used to predict the results are shown by Table 9.

Table 9: relative permeability parameters used to simulate Yousef et al[78] experiments

parameter	Initial value	Final value
1st core flood		
Swc	0.1044	0.1044
Sor	0.33	0.12
Krow	0.8	0.8
Krw	0.5	0.2
nw	2	3
no	2.2	2
2nd core flood		
Swc	0.144	0.144
Sor	0.21	0.08
Krow	0.8	0.8
Krw	0.5	0.2
nw	2	3
no	2.2	2

Figure 25 shows that decreasing salinity of the injection brine increased the calculated wettability indicator (becoming more positive), and shifted the wettability towards water-wet state. It can be observed that the wettability indicator is much increased when the injection brine was switched from SW/2 to SW/10 compared with switching from SW to SW/2. This observation is consistent with the reported oil recovery as SW/2 injection recovered additional 7% OOIP, whereas SW/10 injection produced additional 9.12% OOIP. Injection of the SW/20 further increased the wettability indicator although no significant oil was recovered. It can be suggested that much of the movable oil was retrieved with the earlier injected brines.

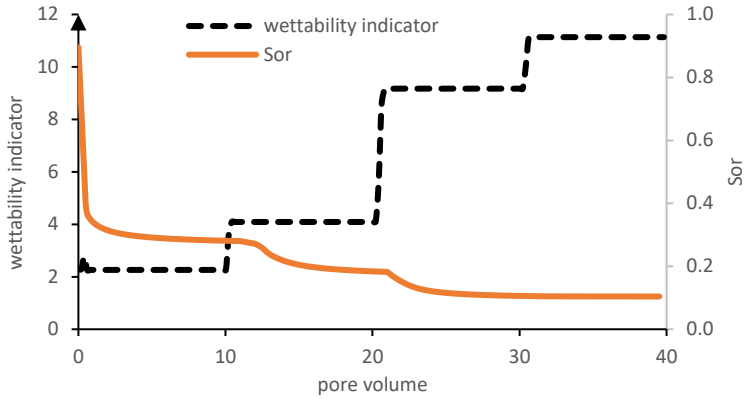

Figure 25: relationship between wettability indicator and residual oil saturation for the various injection cycles (1st core flood).

It can be observed from Figure 26 that the calculated ζ-potentials are positive at the initial condition, which shifted to negative values during SW injection. The rock-brine ζ-potential can be seen to be continuously becoming negative as the diluted brines are injected. During the same injection period, the oil-brine interface also generates negative ζ-potential. This is in consistent with the results reported by the authors in another published paper (Yousef et al[86]). They reported negative ζ-potential at the rock-brine interface when the rock was equilibrated with SW. The ζ-potential then becomes more negative when the SW was diluted ten times, twenty times, and hundred times.

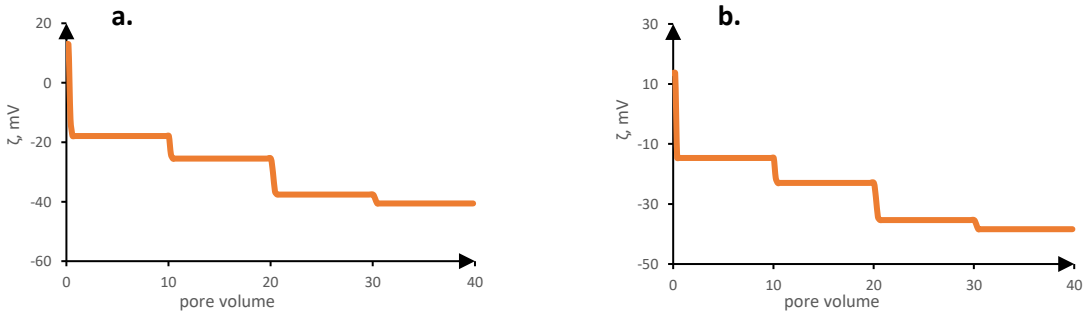

Figure 26: calculated ζ-potential for the COB system. (a) rock-brine ζ-potential, and (b) oil-brine ζ-potential (Yousef et al[78] 1st core flood).

3.4.3. Modelling of Austad et al.[7] CSWF experiments

Austad et al.[7] performed tertiary CSWF in limestone and chalk by injecting FW at secondary stage followed by FW/100 injection. It should be noted that both brines used for the experiment were devoid of SO_4^{-2} ion. Injection of FW through the limestone core produced

65% OOIP, which was increased to 70% OOIP on switching to FW/100. The chalk, on the other hand, recovered 57% OOIP, and switching the injection brine to FW/100 did not recover any additional oil. Austad and colleagues explained that dissolution of anhydrite mineral present in the limestone provided SO_4^{-2} ion, and adsorption of this ion at the rock surface increased oil recovery. They further proposed that the adsorbed SO_4^{-2} co-adsorbed Ca^{+2} and Mg^{+2} leading to the release of adhered oil from the rock surface. We modelled the oil recovery data obtained from the limestone rock with our model (Figure 27). However, regarding the chalk, we qualitatively calculated adhesion number and used it to analyse Austad et al.[7] observations. It is important to note that in simulating the limestone rock, calcite and anhydride dissolution/precipitation reactions were included in the model while only calcite dissolution/precipitation reaction was involved in the chalk rock. Acid site-density (7.52/nm^2) and base site-density (4.51/nm^2) were calculated from the TAN (0.7 mgKOH/g oil) and TBN (0.42 mgKOH/g oil), respectively. We used our capacitances (C1 = 2.84, C1 = 4.48 F/m^2) and carbonate site-densities (4.95/nm^2 for each site) that are used entirely in this paper. Therefore, relative permeability parameters were optimized to match the model to the limestone oil recovery data. The optimized relative permeabilities used to predict the results are shown by Table 10.

Table 10: relative permeability parameters used to simulate Austad et al.[7] limestone experiment

parameter	Initial value	Final value
Swc	0.07	0.07
Sor	0.32	0.28
Krow	0.6	0.6
Krw	0.2	0.2
nw	2	3
no	3	2.5

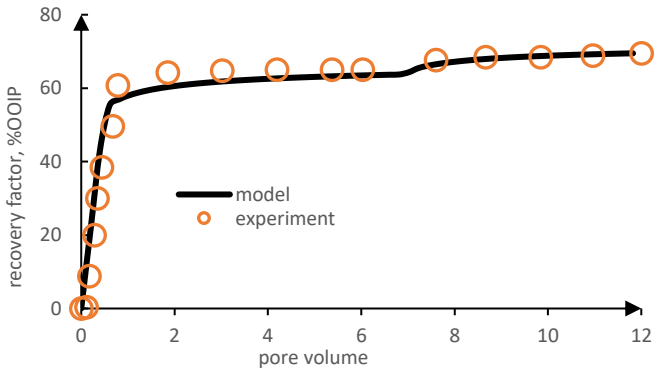

Figure 27: history match of model (this study) to Austad et al.[7] oil recovery data (limestone core).

Figure 28 shows the relationship between the calculated wettability indicator and the residual oil saturation for the limestone rock. The wettability indicator for the FW injection is 1.88, which can be described as weakly water-wet condition. Injection of FW/100 shifted the wettability towards more water-wet state with calculated wettability indicator of 27.5. This increased the oil recovery in the FW/100 injection cycle. Residual oil saturation is observed to reduce further on switching the injection brine to FW/100 brine.

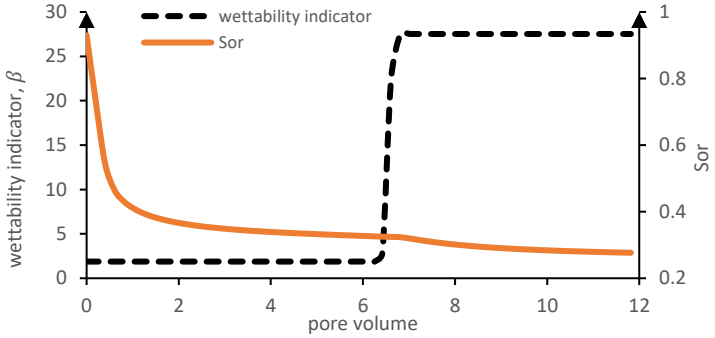

Figure 28: model results of calculated wettability indicator versus residual oil saturation (Austad et al.[7]; limestone).

The model shows positive ζ-potentials calculated at the oil-brine and the rock-brine interfaces during FW injection. However, switching the injection brine to FW/100 produced negative ζ-potentials at both oil-brine and rock-brine interfaces (Figure 29). It can be observed that magnitude of the FW/100 calculated ζ-potentials exceeded FW produced ζ-potentials, generating high repulsive force between the oil and the rock surface. This can be attributed to the additional oil recovered with the FW/100 injection.

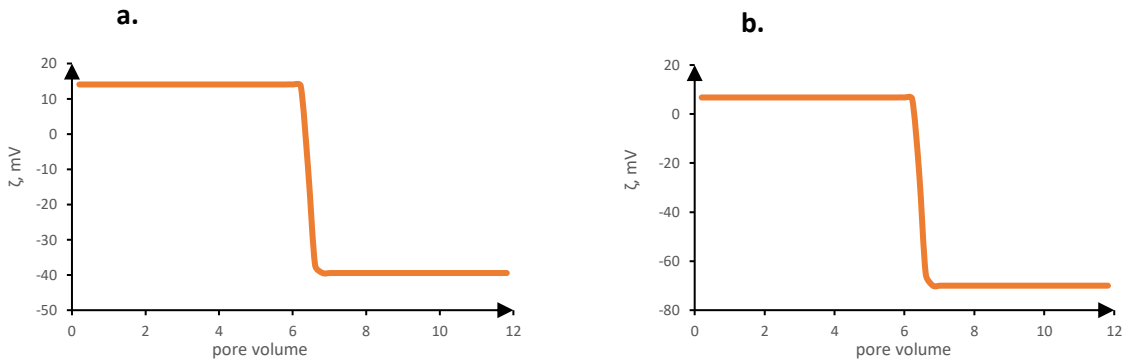

Figure 29: calculated ζ-potential for the COB system. (a) rock-brine ζ-potential; and (b) oil-brine ζ-potential (Austad et al.[7]; limestone rock).

Figure 30 shows the effluent SO_4^{-2} ion concentration during the injection cycle. Both the connate water and the injection brines were devoid of SO_4^{-2} ion, therefore, the produced SO_4^{-2} ion was as a result of anhydrite dissolution. The SO_4^{-2} ion also indicates the amount of dissolved anhydrite. The produced SO_4^{-2} ion concentration is observed to increase when the injection brine was switched to the FW/100 brine, signifying increased anhydrite dissolution. Consequently, the adsorbed SO_4^{-2} ion at the rock surface would increase, shifting the ζ-potential to negative values. The anhydrite dissolution, however, occurred within 1 pore volumes of injection after which equilibrium between the aqueous ions and the mineral was established.

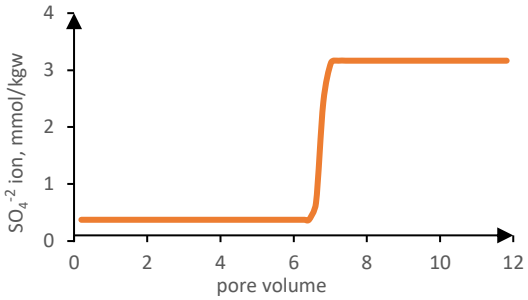

Figure 30: effluent SO_4^{-2} ion

Figure 31 below shows qualitative results of the calculated wettability indicator for the chalk core at the end of each injection period. It can be observed that the wettability indicator at the end of FW injection is 4.23, which reduced to -16.8 following FW/100 injection. This implies increased electrostatic attraction force between the oil and the rock surface, and thus, increased oil adhesion. The authors did not observe additional oil recovery from the FW/100 injection, which can be linked to the increased oil adhesion as observed from the model. They stated that carbonates without SO_4^{-2} (as anhydrite mineral, initially contained in the rock), do not show increased oil recovery with dilution, and this is exactly what the model predicted.

Figure 31: relationship between adhesion number and residual oil saturation (Austad et al.[7]; chalk core).

The calculated ζ-potential for the chalk shows positive ζ-potentials at both oil-brine and rock-brine interfaces during FW injection. Switching the injection brine to FW/100 produced negative ζ-potential at the oil-brine interface, whereas the rock-brine interface still produced positive ζ-potential values (Figure 32).

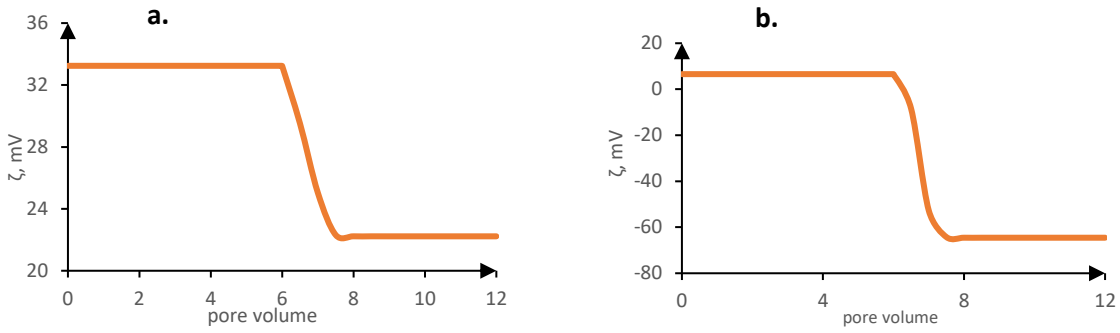

Figure 32: calculated ζ-potential for the COB system. (a) rock-brine ζ-potential; and (b) oil-brine ζ-potential (Austad et al.[7]; chalk core).

3.4.4. Modelling of Sharma & Mohanty.[79] experiments

We also modelled single-phase CSWF results of Sharma & Mohanty[79]. In their experiment, FW was first displaced by SW, which was also displaced by SW4SO4 (i.e.: SW with SO_4^{-2} ion concentration increased four times). We matched the model to the experimental effluent ion concentrations (Figure 33). The experiment was conducted at 120°C; therefore, we optimized the carbonate-brine reactions constants while maintaining capacitances and site-densities values. The obtained equilibrium constants are given in Table 2.

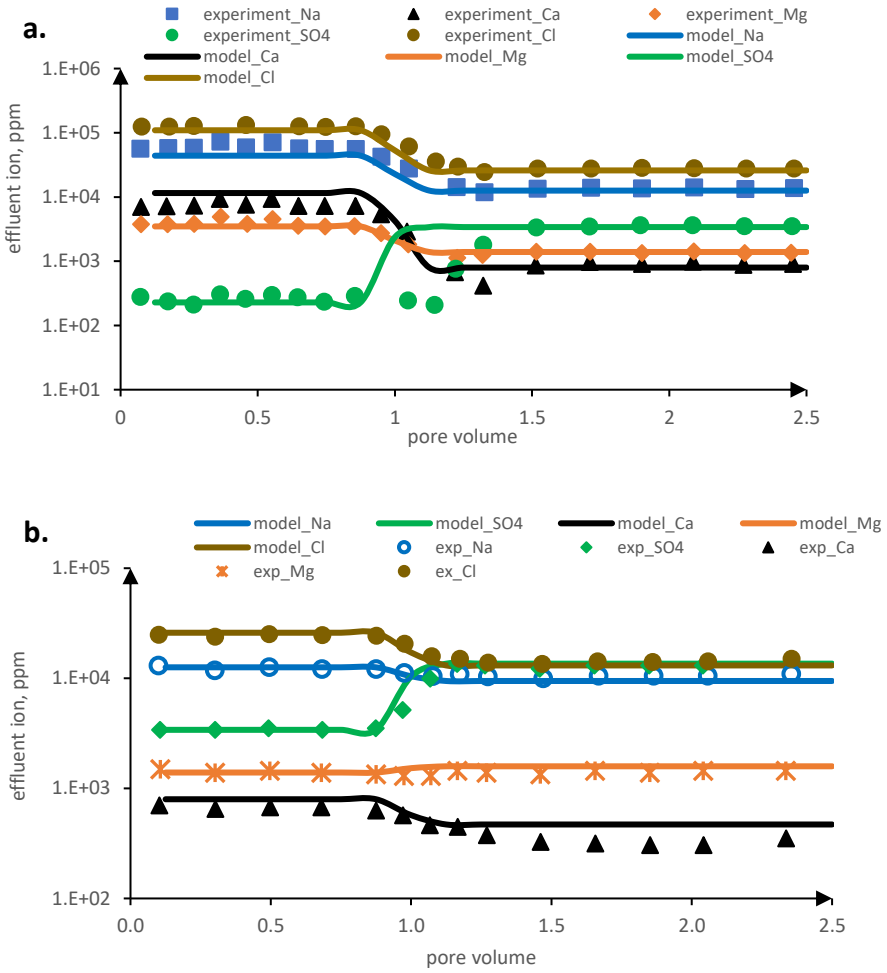

Figure 33: Effluent ion match. (a) SW displacing FW; (b) SW4SO4 displacing SW

4. Conclusions

We presented a triple-layer surface complexation model to characterize carbonate-brine-oil interactions. A wettability indicator based on the ζ-potentials was suggested to offer wettability alteration resulting from brine dilution and/or composition. The developed model was tested against several experimentally measured ζ-potentials and oil recovery data sets. The model offers promising results when used at various conditions of temperature, carbonate mineralogy, brine composition and salinity. Results of the model suggest that:

- Oil basic group significantly impacts oil-brine interface ζ-potential irrespective of temperature, brine composition, and ionic strength.

- Na^+ ions in brine may influence oil-brine ζ-potential, and this relates to temperature, brine composition, and ionic strength.
- Dilutions in chalk tend to shift the reservoir towards oil-wet condition.
- Wettability is related to ζ-potentials at the oil-brine and rock-brine interfaces, and carbonate rock would be strongly oil-wet or water-wet only at significantly large magnitude of ζ-potentials at the interfaces.

Acknowledgments

Authors would like to thank the School of Engineering at the University of Aberdeen for providing required consumables and facilities to complete this research. We also thank Ghana Education Trust Fund (GetFund) for their financial support. The authors would also like to thank Dr Jan Vinogradov at the School of Engineering, University of Aberdeen, for his technical advice.

References

1. Martin, J. The Effects of Clay on the Displacement of Heavy Oil by Water. *3rd Annu. Meet. Soc. Pet. Eng. AIME* 1–24 (1959) doi:10.2118/1411-G.
2. Tang, G. Q. & Morrow, N. R. Salinity, Temperature, Oil Composition, and Oil Recovery by Waterflooding. *SPE Reserv. Eng.* **12**, 269–276 (1997).
3. Morrow, N. R., Tang, G., Valat, M. & Xie, X. Prospects of improved oil recovery related to wettability and brine composition. *J. Pet. Sci. Eng.* **20**, 267–276 (1998).
4. Jadhunandan, P. P. & Morrow, N. R. Effect of Wettability on Waterflood Recovery for Crude-Oil/Brine/Rock Systems. *SPE Reserv. Eng.* **10**, 40–46 (1995).
5. Qiao, C., Johns, R. & Li, L. Understanding the Chemical Mechanisms for Low Salinity Waterflooding. *SPE Eur. Featur. 78th EAGE Conf. Exhib.* (2016) doi:10.2118/180138-MS.
6. Jackson, M. D., Al-Mahrouqi, D. & Vinogradov, J. Zeta potential in oil-water-carbonate systems and its impact on oil recovery during controlled salinity water-flooding. *Sci. Rep.* **6**, (2016).
7. Austad, T., Shariatpanahi, S. F., Strand, S., Black, C. J. J. & Webb, K. J. Conditions for a low-salinity Enhanced Oil Recovery (EOR) effect in carbonate oil reservoirs. *Energy and Fuels* **26**, 569–575 (2012).
8. Lager, A., Webb, K. J., Black, C. J. J., Singleton, M. & Sorbie, K. S. Low Salinity Oil Recovery - An Experimental Investigation. 0–12 (2008) doi:SPWLA-2008-v49n1a2.
9. Alshakhs, M. J. & Kovscek, A. R. Understanding the role of brine ionic composition on oil recovery by assessment of wettability from colloidal forces. *Adv. Colloid Interface Sci.* **233**, 126–138 (2016).
10. Awolayo, A. N., Sarma, H. K. & Nghiem, L. X. Modeling the characteristic thermodynamic interplay between potential determining ions during brine-dependent recovery process in carbonate rocks. *Fuel* **224**, 701–717 (2018).
11. Buckley, J. S., Morrow, N. R. & Takamura, J. Influence of electrical surface charges on the wetting properties of crude oils. 332–340 (1987).
12. Xie, Q., Saeedi, A., Pooryousefy, E. & Liu, Y. Extended DLVO-based estimates of surface force in low salinity water flooding. *J. Mol. Liq.* **221**, 658–665 (2016).
13. Fathi, S. J., Austad, T. & Strand, S. 'smart water' as a wettability modifier in chalk: The effect of salinity and ionic composition. *Energy and Fuels* **24**, 2514–2519 (2010).
14. Strand, S., Høgnesen, E. J. & Austad, T. Wettability alteration of carbonates - Effects of potential determining ions (Ca2+and SO42-) and temperature. *Colloids Surfaces A*

Physicochem. Eng. Asp. **275**, 1–10 (2006).
15. Zhang, P., Tweheyo, M. T. & Austad, T. Wettability alteration and improved oil recovery by spontaneous imbibition of seawater into chalk: Impact of the potential determining ions Ca2+, Mg2+, and SO42-. *Colloids Surfaces A Physicochem. Eng. Asp.* **301**, 199–208 (2007).
16. Zhang, P. & Austad, T. Wettability and oil recovery from carbonates: Effects of temperature and potential determining ions. *Colloids Surfaces A Physicochem. Eng. Asp.* **279**, 179–187 (2006).
17. Hiorth, A. & Evje, S. A mathematical model for dynamic wettability alteration controlled by water-rock chemistry. *Networks Heterog. Media* **5**, 217–256 (2010).
18. Omekeh, A. V., Friis, H. A., Fjelde, I. & Evje, S. Modeling of Ion-Exchange and Solubility in Low Salinity Water Flooding. *SPE Improv. Oil Recover. Symp.* (2012) doi:10.2118/154144-MS.
19. McGuire, P. L., Chatham, J. R., Paskvan, F. K., Sommer, D. M. & Carini, F. H. Low Salinity Oil Recovery: An Exciting New EOR Opportunity for Alaska's North Slope. *SPE West. Reg. Meet.* 1–15 (2005) doi:10.2118/93903-MS.
20. Doust, A. R., Puntervold, T. & Austad, T. Chemical verification of the EOR mechanism by using low saline/smart water in sandstone. *Energy and Fuels* **25**, 2151–2162 (2011).
21. Puntervold, T., Strand, S. & Austad, T. Water flooding of carbonate reservoirs: Effects of a model base and natural crude oil bases on chalk wettability. *Energy and Fuels* **21**, 1606–1616 (2007).
22. Zhang, Y. & Sarma, H. Improving waterflood recovery efficiency in carbonate reservoirs through salinity variations and ionic exchanges: A promising low-cost 'smart-waterflood' approach. *Abu Dhabi Int. Pet. Exhib. Conf. 2012 - Sustain. Energy Growth People, Responsib. Innov. ADIPEC 2012* **3**, 2163–2183 (2012).
23. Hiorth, A., Cathles, L. M. & Madland, M. V. The Impact of Pore Water Chemistry on Carbonate Surface Charge and Oil Wettability. *Transp. Porous Media* **85**, 1–21 (2010).
24. Mahani, H. *et al.* Insights into the mechanism of wettability alteration by low-salinity flooding (LSF) in carbonates. *Energy and Fuels* **29**, 1352–1367 (2015).
25. Mahani, H., Keya, A. L., Berg, S. & Nasralla, R. Electrokinetics of Carbonate/Brine Interface in Low-Salinity Waterflooding: Effect of Brine Salinity, Composition, Rock Type, and pH on ζ-Potential and a Surface-Complexation Model. *SPE J.* **22**, 053–068 (2017).
26. Romanuka, J. *et al.* Low Salinity EOR in Carbonates. *SPE Improv. Oil Recover. Symp.* (2012) doi:10.2118/153869-MS.
27. AlQuraishi, A. A., Alhussinan, S. N., Alyami, H. Q. & Abdulaziz, K. Efficiency and Recovery Mechanisms of Low Salinity Water Flooding in Sandstone and Carbonate Reservoirs. *12th Offshore Mediterr. Conf. Exhib.* 1–14 (2015).
28. AlSada, A. & Mackay, E. Low Salinity Water Flooding Possible Mechanisms and the Impact of Injected Sulphate Variation on Oil Recovery in Carbonate Reservoirs: Compositional Modelling Approach. *SPE Kingdom Saudi Arab. Annu. Tech. Symp. Exhib.* (2017) doi:10.2118/187980-MS.
29. Al Mahrouqi, D., Vinogradov, J. & Jackson, M. D. Zeta potential of artificial and natural calcite in aqueous solution. *Adv. Colloid Interface Sci.* **240**, 60–76 (2017).
30. Wolthers, M., Charlet, L. & Van Cappellen, P. The surface chemistry of divalent metal carbonate minerals: A critical assessment of surface charge and potential data using the charge distribution multi-site ion complexation model. *Am. J. Sci.* **308**, 905–941 (2008).

31. Hirasaki, G. J. Wettability: Fundamentals and Surface Forces. *SPE Form. Eval.* **6**, 217–226 (1991).
32. Qiao, C., Johns, R. & Li, L. Modeling Low-Salinity Waterflooding in Chalk and Limestone Reservoirs. *Energy and Fuels* **30**, 884–895 (2016).
33. Chandrasekhar, S., Sharma, H. & Mohanty, K. K. Dependence of wettability on brine composition in high temperature carbonate rocks. *Fuel* **225**, 573–587 (2018).
34. Gopani, P. H., Singh, N., Sarma, H. K., Mattey, P. & Srivastava, V. R. Role of Monovalent and Divalent Ions in Low-Salinity Water Flood in Carbonate Reservoirs: An Integrated Analysis through Zeta Potentiometric and Simulation Studies. *Energies* **14**, 729 (2021).
35. Bordeaux-Rego, F., Mehrabi, M., Sanaei, A. & Sepehrnoori, K. Improvements on modelling wettability alteration by Engineered water injection: Surface complexation at the oil/brine/rock contact. *Fuel* **284**, 118991 (2021).
36. Elakneswaran, Y., Shimokawara, M., Nawa, T. & Takahashi, S. Surface complexation and equilibrium modelling for low salinity waterflooding in sandstone reservoirs. *Soc. Pet. Eng. - SPE Abu Dhabi Int. Pet. Exhib. Conf. 2017* **2017-Janua**, (2017).
37. Takeya, M., Shimokawara, M., Elakneswaran, Y., Nawa, T. & Takahashi, S. Predicting the electrokinetic properties of the crude oil/brine interface for enhanced oil recovery in low salinity water flooding. *Fuel* **235**, 822–831 (2019).
38. Takeya, M. *et al.* Crude oil/brine/rock interface in low salinity waterflooding: Experiments, triple-layer surface complexation model, and DLVO theory. *J. Pet. Sci. Eng.* **188**, 106913 (2020).
39. Brady, P. V. & Thyne, G. Functional Wettability in Carbonate Reservoirs. *Energy and Fuels* **30**, 9217–9225 (2016).
40. Brady, P. V., Krumhansl, J. L. & Mariner, P. E. Surface complexation modeling for improved oil recovery. *Proc. - SPE Symp. Improv. Oil Recover.* **1**, 376–385 (2012).
41. Bonto, M., Eftekhari, A. A. & Nick, H. A calibrated model for the carbonate-brine-crude oil surface chemistry and its effect on the rock wettability, dissolution, and mechanical properties. *Soc. Pet. Eng. - SPE Reserv. Simul. Conf. 2019, RSC 2019* (2019) doi:10.2118/193865-ms.
42. Bonto, M., Eftekhari, A. A. & Nick, H. M. An overview of the oil-brine interfacial behavior and a new surface complexation model. *Sci. Rep.* **9**, 1–16 (2019).
43. Kazemi Nia Korrani, A., Sepehrnoori, K. & Delshad, M. Coupling IPhreeqc with UTCHEM to model reactive flow and transport. *Comput. Geosci.* **82**, 152–169 (2015).
44. Korrani, A. K. N. & Jerauld, G. R. Modeling wettability change in sandstones and carbonates using a surface-complexation-based method. *J. Pet. Sci. Eng.* **174**, 1093–1112 (2019).
45. Sanaei, A., Varavei, A. & Sepehrnoori, K. Mechanistic modeling of carbonated waterflooding. *Proc. - SPE Symp. Improv. Oil Recover.* **2018-April**, (2018).
46. Walid Al Shalabi, E. & Sepehrnoori, K. Modeling of the LSWI/EWI Technique in Sandstones and Carbonates. *Low Salin. Eng. Water Inject. Sandstone Carbonate Reserv.* 51–71 (2017) doi:10.1016/B978-0-12-813604-1.00005-5.
47. Polanska, A., Asen, S., Omekeh, A. & Fjelde, I. Secondary and Tertiary Low Salinity Water Floods: Experiments and Modeling. *75th EAGE Conf. Exhib. …* (2013) doi:10.2118/164920-MS.
48. Xie, Q. *et al.* pH effect on wettability of oil/brine/carbonate system: Implications for low salinity water flooding. *J. Pet. Sci. Eng.* **168**, 419–425 (2018).
49. GOLDBERG, S. Surface complexation modeling.
50. Luo, H., Al-Shalabi, E. W., Delshad, M., Panthi, K. & Sepehrnoori, K. A Robust Geochemical Simulator To Model Improved-Oil-Recovery Methods. *SPE J.* **21**, 055–

073 (2016).
51. Kazemi Nia Korrani, A., Sepehrnoori, K. & Delshad, M. A comprehensive geochemical-based approach to quantify the scale problems. *SPE - Eur. Form. Damage Conf. Proceedings, EFDC* **2**, 946–964 (2014).
52. Erzuah, S., Fjelde, I. & Omekeh, A. V. Wettability estimation using surface-complexation simulations. *SPE Reserv. Eval. Eng.* **22**, 509–519 (2019).
53. Israelachvili, J. N. *Electrostatic Forces between Surfaces in Liquids*. *Intermolecular and Surface Forces* (2011). doi:10.1016/b978-0-12-375182-9.10014-4.
54. Heberling, F. *et al.* Reactivity of the calcite-water-interface, from molecular scale processes to geochemical engineering. *Appl. Geochemistry* **45**, 158–190 (2014).
55. Heberling, F. *et al.* Structure and reactivity of the calcite-water interface. *J. Colloid Interface Sci.* **354**, 843–857 (2011).
56. Rahnemaie, R., Hiemstra, T. & Van Riemsdijk, W. H. A new surface structural approach to ion adsorption: Tracing the location of electrolyte ions. *J. Colloid Interface Sci.* **293**, 312–321 (2006).
57. Hiemstra, T. & Van Riemsdijk, W. H. A surface structural approach to ion adsorption: The charge distribution (CD) model. *J. Colloid Interface Sci.* **179**, 488–508 (1996).
58. Sø, H. U., Postma, D., Jakobsen, R. & Larsen, F. Competitive adsorption of arsenate and phosphate onto calcite; experimental results and modeling with CCM and CD-MUSIC. *Geochim. Cosmochim. Acta* **93**, 1–13 (2012).
59. Sø, H. U. *Adsorption of arsenic and phosphate onto the surface of calcite as revealed by batch experiments and surface complexation modelling*. (2011). doi:10.13140/2.1.1196.1603.
60. Tadanier, C. J. & Eick, M. J. Formulating the Charge-distribution Multisite Surface Complexation Model Using FITEQL. *Soil Sci. Soc. Am. J.* **66**, 1505–1517 (2002).
61. Stipp, S. L. S. Toward a conceptual model of the calcite surface: Hydration, hydrolysis, and surface potential. *Geochim. Cosmochim. Acta* **63**, 3121–3131 (1999).
62. Brady, P. V. & Krumhansl, J. L. Surface complexation modeling for waterflooding of sandstones. *SPE J.* **18**, 214–218 (2013).
63. Brady, P. V. & Krumhansl, J. L. A surface complexation model of oil-brine-sandstone interfaces at 100°C: Low salinity waterflooding. *J. Pet. Sci. Eng.* **81**, 171–176 (2012).
64. Korrani, A. K. N. & Jerauld, G. R. Modeling wettability change in sandstones and carbonates using a surface-complexation-based method. *J. Pet. Sci. Eng.* **174**, 1093–1112 (2019).
65. Eftekhari, A. A., Thomsen, K., Stenby, E. H. & Nick, H. M. Thermodynamic Analysis of Chalk-Brine-Oil Interactions. *Energy and Fuels* **31**, 11773–11782 (2017).
66. Rahnemaie, R., Hiemstra, T. & van Riemsdijk, W. H. Inner- and outer-sphere complexation of ions at the goethite-solution interface. *J. Colloid Interface Sci.* **297**, 379–388 (2006).
67. Van Cappellen, P., Charlet, L., Stumm, W. & Wersin, P. A surface complexation model of the carbonate mineral-aqueous solution interface. *Geochim. Cosmochim. Acta* **57**, 3505–3518 (1993).
68. Li, S. *et al.* Influence of surface conductivity on the apparent zeta potential of calcite. *J. Colloid Interface Sci.* **468**, 262–275 (2016).
69. Song, J. *et al.* Surface complexation modeling of calcite zeta potential measurements in brines with mixed potential determining ions (Ca2+, CO32−, Mg2+, SO42−) for characterizing carbonate wettability. *J. Colloid Interface Sci.* **506**, 169–179 (2017).
70. Brady, P. V. & Krumhansl, J. L. A surface complexation model of oil-brine-sandstone interfaces at 100°C: Low salinity waterflooding. *J. Pet. Sci. Eng.* **81**, 171–176 (2012).
71. Delshad, M., Pope, G. A. & Sepehrnoori, K. A compositional simulator for modeling

surfactant enhanced aquifer remediation, 1 Formulation. *J. Contam. Hydrol.* **23**, 303–327 (1996).
72. Parkhurst, D. L. & Wissmeier, L. PhreeqcRM: A reaction module for transport simulators based on the geochemical model PHREEQC. *Adv. Water Resour.* **83**, 176–189 (2015).
73. Nia Korrani, A. K., Sepehrnoori, K. & Delshad, M. A novel mechanistic approach for modeling low salinity water injection. *SPE Annu. Tech. Conf. Proc.* **7**, 3206–3223 (2013).
74. Korrani, A. K. N., Sepehrnoori, K. & Delshad, M. A mechanistic integrated geochemical and chemical-flooding tool for alkaline/surfactant/polymer floods. *SPE J.* **21**, 32–54 (2016).
75. Parkhurst, B. D. L. User ' s Guide to PHREEQC — a Computer Program for Inverse Geochemical Calculations. (1995).
76. Ding, H., Mettu, S. & Rahman, S. Probing the Effects of Ca2+, Mg2+, and SO42-on Calcite-Oil Interactions by 'soft Tip' Atomic Force Microscopy (AFM). *Ind. Eng. Chem. Res.* **59**, 13069–13078 (2020).
77. Goldberg, S. Modeling Selenite Adsorption Envelopes on Oxides, Clay Minerals, and Soils using the Triple Layer Model. *Soil Sci. Soc. Am. J.* **77**, 64–71 (2013).
78. Yousef, A. A., Al-Saleh, S., Al-Kaabi, A. & Al-Jawfi, M. Laboratory investigation of novel oil recovery method for carbonate reservoirs. *Soc. Pet. Eng. - Can. Unconv. Resour. Int. Pet. Conf. 2010* **3**, 1825–1859 (2010).
79. Sharma, H. & Mohanty, K. K. An experimental and modeling study to investigate brine-rock interactions during low salinity water flooding in carbonates. *J. Pet. Sci. Eng.* **165**, 1021–1039 (2018).
80. Lu, Y., Najafabadi, N. F. & Firoozabadi, A. Effect of Temperature on Wettability of Oil/Brine/Rock Systems. *Energy and Fuels* **31**, 4989–4995 (2017).
81. Chow, R. S. & Takamura, K. Electrophoretic mobilities of bitumen and conventional crude-in-water emulsions using the laser Doppler apparatus in the presence of multivalent cations. *J. Colloid Interface Sci.* **125**, 212–225 (1988).
82. Awolayo, A., Sarma, H. & AlSumaiti, A. M. A laboratory study of ionic effect of smart water for enhancing oil recovery in carbonate reservoirs. *Soc. Pet. Eng. - SPE EOR Conf. Oil Gas West Asia 2014 Driv. Integr. Innov. EOR* 46–69 (2014) doi:10.2118/169662-ms.
83. Parkhurst, D. L. & Appelo, C. a. J. Description of Input and Examples for PHREEQC Version 3 — A Computer Program for Speciation , Batch-Reaction , One-Dimensional Transport , and Inverse Geochemical Calculations. U.S. Geological Survey Techniques and Methods, book 6, chapter A43, 497 p. *U.S. Geol. Surv. Tech. Methods, B. 6, chapter A43* 6-43A (2013).
84. Korrani, A. K. N. Mechanistic Modeling of Low Salinity Water Injection. 685 (2014).
85. Smallwood, P. V. Some aspects of the surface chemistry of calcite and aragonite - Part II: Crystal growth. *Colloid Polym. Sci. Kolloid-Zeitschrift Zeitschrift für Polym.* **255**, 994–1000 (1977).
86. Yousef, A. A., Al-Saleh, S. & Al-Jawfi, M. Improved/enhanced oil recovery from carbonate reservoirs by tuning injection water salinity and ionic content. *Proc. - SPE Symp. Improv. Oil Recover.* **1**, 819–836 (2012).